

LEVEL

12



RADC-TR-79-51
Final Technical Report
April 1979

AD A 069623

SECURE OPTICAL MATRIX SWITCH

Sperry Research Center

Richard A. Soref



APPROVED FOR PUBLIC RELEASE; DISTRIBUTION UNLIMITED

DDC FILE COPY,

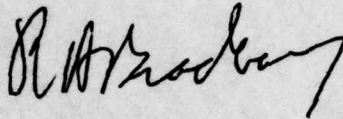
ROME AIR DEVELOPMENT CENTER
Air Force Systems Command
Griffiss Air Force Base, New York 13441

79 06 08 010

This report has been reviewed by the RADC Information Office (OI) and is releasable to the National Technical Information Service (NTIS). At NTIS it will be releasable to the general public, including foreign nations.

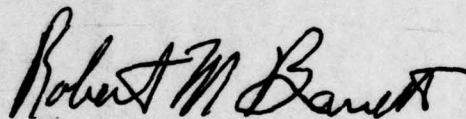
RADC-TR-79-51 has been reviewed and is approved for publication.

APPROVED:



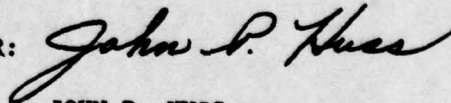
RUDOLPH BRADBURY
Project Engineer

APPROVED:



ROBERT M. BARRETT, Director
Solid State Sciences Division

FOR THE COMMANDER:



JOHN P. HUSS
Acting Chief, Plans Office

If your address has changed or if you wish to be removed from the RADC mailing list, or if the addressee is no longer employed by your organization, please notify RADC (ESO), Hanscom AFB MA 01730. This will assist us in maintaining a current mailing list.
Do not return this copy. Retain or destroy.

UNCLASSIFIED

SECURITY CLASSIFICATION OF THIS PAGE (When Data Entered)

7076

REPORT DOCUMENTATION PAGE		READ INSTRUCTIONS BEFORE COMPLETING FORM
1. REPORT NUMBER RADC-TR-79-51	2. GOVT ACCESSION NO. TR-79-54	3. RECIPIENT'S CATALOG NUMBER
4. TITLE (and Subtitle) SECURE OPTICAL MATRIX SWITCH	5. TYPE OF REPORT & PERIOD COVERED Final Technical Report 15 June 77 - 15 June 78	6. PERFORMING ORG. REPORT NUMBER CR-78-35
7. AUTHOR(s) Richard A./Soref	8. CONTRACT OR GRANT NUMBER(s) F19628-77-C-0187	
9. PERFORMING ORGANIZATION NAME AND ADDRESS Sperry Research Center 100 North Road Sudbury MA 01776	10. PROGRAM ELEMENT, PROJECT, TASK AREA & WORK UNIT NUMBERS 62702F 46001921	
11. CONTROLLING OFFICE NAME AND ADDRESS Deputy for Electronic Technology (RADC/ESO) Hanscom AFB MA 01731	12. REPORT DATE April 1979	
14. MONITORING AGENCY NAME & ADDRESS (if different from Controlling Office) Same	13. NUMBER OF PAGES 105	
14. MONITORING AGENCY NAME & ADDRESS (if different from Controlling Office) Same	15. SECURITY CLASS. (of this report) UNCLASSIFIED	
16. DISTRIBUTION STATEMENT (of this Report) Approved for public release; distribution unlimited.	15a. DECLASSIFICATION/DOWNGRADING SCHEDULE N/A	
17. DISTRIBUTION STATEMENT (of the abstract entered in Block 20, if different from Report) Same		
18. SUPPLEMENTARY NOTES RADC Project Engineer: Rudolph A. Bradbury (ESO)		
19. KEY WORDS (Continue on reverse side if necessary and identify by block number)		
optical switching	optical matrix	insertion loss
fiber optics	crossbar switching	coupling
electrooptic devices	connecting networks	waveguides
lithium tantalate	multimode fibers	light emitting diodes
communication system	crosstalk	
20. ABSTRACT (Continue on reverse side if necessary and identify by block number)		
<p>Novel fiber-optic switching arrays have been developed to control the network configuration of a secure fiber-optic intercom system. A fiber-linked system containing six optical data terminals was built and has been matrix-switched by a multimode 3 x 2 array constructed in an 80-μm-thick single-crystal LiTaO₃ plate. Commercial multimode 0.15NA fibers, 85-μm core diameter, have been directly and permanently coupled to the plate ends at the matrix input and output ports, one strand for each data channel. Using oblique incidence, (Cont'd)</p>		

DD FORM 1 JAN 73 1473

408 199

UNCLASSIFIED

SECURITY CLASSIFICATION OF THIS PAGE (When Data Entered)

Item 20 (Cont'd)

the fiber light cone was collimated by a factor of 2.6 in the crystal. The optical data sources consisted of GaAs LEDs emitting at the 0.90 μ m wavelength. Electrically controlled optical switching has been obtained with unpolarized TE- and TM-mode light launched in the crystal.

The matrix or "crossbar" is an assemblage of four-port switches or "crosspoints" that deflect multimode light by means of the Pockel's effect. Each crosspoint consists of a voltage-controlled reflection element situated at the 3.6° - intersection of two electrooptic channels (3-d waveguides induced in the crystal by continuous bias voltage).

Initial tests were made on a 2 x 2 crossbar coupled to convergent 0.63- μ m laser beams. This was the first multimode crossbar reported in the literature. An optical insertion loss of 11 dB and an optical crosstalk level of -16dB were observed for the fully addressed crossbar with TM-polarized input light having an 0.07 NA.

Finally, the fiber-coupled crossbar, the first switch of its kind, was built. Here, the number of channels was increased to six and the number of independent crosspoints was increased to nine within the 6.6 cm x 1.0 cm crossbar area. Tests carried out in the above intercom showed that this crossbar had a 19 dB insertion loss and an -8 dB extinction ratio with addressing voltages in the 400 to 500 V range and a 19 pF crosspoint capacitance. Improvements of 3 dB in the throughput and crosstalk performance are believed feasible. Problems were encountered in maintaining adequate insulation between the waveguide electrodes and the conductive paths going to the crosspoints.

Accession For	
NTIS GRA&I	<input checked="checked" type="checkbox"/>
DDC TAB	<input type="checkbox"/>
Unannounced	<input type="checkbox"/>
Justification	
By _____	
Distribution/ _____	
Availability Codes	
Dist	Available for special
A	

UNCLASSIFIED

TABLE OF CONTENTS

<u>Section</u>		<u>Page</u>
1	INTRODUCTION	1
2	ELECTROOPTIC APPROACH	2
3	THE OPTICAL MATRIX	6
	A. Definitions	6
	B. Addressing	9
	C. Configurations	9
	D. Duplexing	9
	E. Optical Crosstalk Theory	13
	F. Fiber Coupling	13
	G. Optical Insertion Loss Theory	14
	H. Fiber Optic Intercom System	16
4	THE CROSSPOINTS	16
	A. Design and Results	16
	B. Theory	20
	C. Comparison	29
	D. Passive Effect	29
5	THE 2 X 2 MATRIX SWITCH	29
	A. Design	29
	B. Results	37
6	DESIGN OF 3 X 3 MATRIX SWITCH	37
7	TECHNIQUES FOR DEVICE FABRICATION	41
8	YIELD PROBLEM ON 3 X 3 MATRICES	47
	A. Experimental Crystals	48
9	FIBER ARRAY TERMINATIONS	51
10	CONTROL ELECTRONICS	54
11	OPTICAL DATA TERMINALS	58
	A. Transmitters	58
	B. Receivers	58
12	EXPERIMENTAL RESULTS ON 3 X 3 SYSTEM	64
	A. Assembly of fiber-matrix-fiber combination	64
	B. Performance measurements	68

TABLE OF CONTENTS (Cont.)

<u>Section</u>		<u>Page</u>
13	DISCUSSION	72
14	SUMMARY AND CONCLUSIONS	79
15	RECOMMENDATIONS FOR FUTURE WORK	81
	REFERENCES	85
	APPENDIX A: Device Processing Procedure	86
	APPENDIX B: Bibliography	92

LIST OF ILLUSTRATIONS

<u>Figure</u>		<u>Page</u>
1	Induced index perturbation in LiNbO_3 and LiTaO_3 as a function of applied field.	4
2	Critical angle in LiNbO_3 and LiTaO_3 as a function of applied field.	5
3	Ideal states of crosspoint.	7
4	Actual states of multimode crosspoint.	7
5	Topology of permutation matrix and crossbar matrix.	8
6	Topology of rectangular matrix and one-sided matrix.	10
7	Six possible configurations of 3 X 3 optical matrix.	11
8	Duplex communication in matrix switched network.	12
9	Coupling of input and output fibers at off-normal incidence to crystalline matrix.	15
10	Theoretical dependence of fiber and crystal end-fire-coupling angles upon optical collimation factor.	15
11	General system diagram for switched fiber-optic intercom.	18
12	Specific features of the six-terminal crossbar-switched system delivered to RADC/ET.	18
13	Layout of four-port reflective crosspoint device.	19
14	Two methods of deflecting light in a crossbar.	21
15	Refractive crosspoint device.	22
16	Observed performance of refraction crosspoint A.	23
17	Observed performance of refraction crosspoint B.	24
18	Observed performance of reflection crosspoint.	25
19	Top view of reflection crosspoint that defines angles of switched light rays, incident rays, and channel intersection.	26

LIST OF ILLUSTRATIONS (Cont.)

<u>Figure</u>		<u>Page</u>
20	Calculated values of switched optical power for Fig. 13 crosspoint as a function of input light cone angle.	28
21	Electrode layout in photoresist mask 2 X 2 -1 for top surface of matrix crystal.	31
22	Electrode layout in photoresist mask 2 X 2 -2 for bottom surface matrix crystal.	32
23	Detail of crosspoints in Fig. 21 matrix.	33
24	Detail of crosspoint region in Fig. 22 ground plane.	34
25	Photoresist window-mask 2 X 2 -3 for making electrical contact to crosspoints and channel boundaries.	35
26	Metal evaporation mask 2 X 2 -4 for making conductive fan-outs.	36
27	Experimental model of multimode 2 X 2 optical crossbar matrix.	38
28	Enlarged view of optical switching region of matrix.	39
29	Measurements of switched optical power in 2 X 2 crossbar as a function of crosspoint addressing voltage.	40
30	Photoresist mask 3 X 3 -1 for top-surface electrode pattern of crossbar.	42
31	Photoresist mask 3 X 3 -2 for bottom-surface electrode pattern of crossbar.	43
32	Photoresist mask 3 X 3 -3 for making openings in insulating film covering 3 X 3 top-electrode pattern.	44
33	Metal evaporation mask 3 X 3 -4 for laying down gold paths that enter the Fig. 32 windows.	45
34	End view of optical matrix.	46
35	Exploded view of angle-terminated matrix illustrating how the device is put together.	46
36	Matrix crystal (3 X 3 sample 10) in which the desired processing via masks 1-4 has been carried out on both sides.	49

LIST OF ILLUSTRATIONS (Cont.)

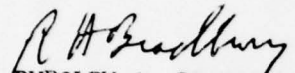
<u>Figure</u>		<u>Page</u>
37	Experimental model of completely processed multimode optical matrix (3 X 3 sample 10).	49
38	Two views of 3-fiber arrays showing how the angle-termination is done simultaneously on two arrays.	52
39	Magnified end-views of actual 3-fiber arrays, input and output trios, terminated at 72° to the fiber axes.	53
40	Top view of terminated fiber arrays, ready for matrix coupling.	53
41	Block diagram of optical matrix control box including self-contained power supplies.	55
42	Circuit diagram of 3 X 3 optical matrix control box showing all five-volt switching circuits.	56
43	Remainder of control box: transistor switching circuits and associated power supply for controlling optical crosspoints.	57
44	Two views of 3 X 3 matrix control box showing keyboard, backpanel adjustments, and 11-wire connector.	59
45	Circuit diagram of optical transmitters for intercom system.	60
46	Inside view of experimental 3-terminal box containing independents GaAs LED data sources.	61
47	Multiple sources for optical intercom system.	62
48	Circuit diagram of optical receivers for intercom system.	63
49	Inside view of experimental 3-terminal box containing independent infrared detector/preamps and digital signal-processing circuits.	65
50	Multiple receivers for optical intercom system.	66
51	Experimental model of multimode 3 X 2 fiber-optical-matrix switch including electrical control wires.	67
52	Switched optical outputs from three fibers coupled to 3 X 2 matrix sample 8.	69

LIST OF ILLUSTRATIONS (Cont.)

<u>Figure</u>		<u>Page</u>
53	Experimental multimode six-terminal crossbar-switched fiber-optic intercom system delivered to RADC/ETSL.	71
54	Modulated 0.90 μm light from each of the GaAs LED sources.	71
55	Experimental performance of 3 X 2 fiber/matrix/fiber system (sample 8) excited by TE+TM 0.90 μm LED light, with terminals 1 and 3 transmitting.	74
56	Experimental performance of 3 X 3 fiber/matrix/fiber system (sample 8) excited by TE+TM 0.90 μm LED light, with terminal 2 transmitting.	75
57	Experimental performance of 3 X 2 fiber/matrix/fiber system (sample 8) excited by TE+TM 0.90 μm LED light, with terminal 3 transmitting.	76
<u>Table</u>		<u>Page</u>
1	Theoretical loss components in dB for addressed 3 X 3 matrix.	17
2	Status of ten 3 X 3 matrix devices prepared in LiTaO ₃ crystals.	50
3	Measured performance of angle-coupled fiber/matrix/fiber switch.	73

EVALUATION

This report is the Final Report on the contract titled Secure Optical Matrix Switch. A 3X3 multimode optical crossbar matrix switch has been designed and constructed. This work demonstrates the feasibility of using optical non-linear materials for coupling together a matrix of optical multimode fibers. These studies are of value since they provide a basis for determining the extent to which these techniques may be used for the solution of Air Force Communication problems.


RUDOLPH A. BRADBURY
Project Engineer

SECURE OPTICAL MATRIX SWITCH

1. INTRODUCTION

The goals of this contract are to investigate the optical design of a secure optical matrix switch and to fabricate and prove feasibility of a 3 x 3 optical matrix. This multimode switching array will interface with six strands of multimode fiber, one strand for each information channel. Three optical terminals are to communicate over all possible interconnection paths with a second group of three terminals.

Two of the applications envisioned for the matrix are (1) a network control switch in a high-security fiber optic intercom system and (2) a central control switch for an optically linked distributed computer. Commercially available LiTaO_3 crystalline materials have been employed in an all-electro-optic approach. Voltage controlled structures for optical waveguiding and switching have been created in the electro-optic substrate.

The subcomponents of the matrix are four-port optical tapoff switches known as "crosspoints". Several crosspoints have been joined monolithically with connecting waveguides into a special kind of matrix called an "optical crossbar".

Tasks on the contract were divided into four areas: (1) optimization of crosspoints, (2) construction of a laser-coupled 2 x 2 crossbar, (3) construction of a fiber-coupled 3 x 3 crossbar and (4) assembly and test of a complete matrix-switched, six-terminal communication system utilizing commercial 0.15 NA fibers, infrared LED sources, and pin diode receivers. Complete support electronics are to be provided with the system, while a low insertion loss and low crosstalk are sought for the matrix.

This Final Report covers the work carried out in a one-year effort beginning June 1977. Most of the contract goals have been met, and the operational keyboard-controlled system has been delivered to RADC/ETSL. Under this contract, the first multimode fiber-coupled matrices have been developed.

The planar monolithic optical circuits are novel and contain a large number of optical elements.

This Report begins with background information on the electro-optic approach and matrix design (Secs. 2 and 3). Following this, the crosspoint results are summarized and compared to theory (Sec. 4). Section 5 gives fabrication and test results on the 2 x 2 matrix, while Sec. 6 spells out how the 3 x 3 array was designed. Fabrication methods are discussed in Sec. 7.

Section 8 describes problems that were encountered during processing of the 3 x 3 crystals, and the next three sections (Secs. 9, 10 and 11) cover some "hardware" aspects of the system, including optical terminals, matrix controller, and fiber terminations.

Our findings on the experimental intercom system are set forth in Sec. 12, and the results are then discussed and analyzed in Sec. 13. The Report concludes with a summary (Sec. 14) and recommendations for future work (Sec. 15).

2. ELECTRO-OPTIC APPROACH

This approach proved successful in the previous contract¹ and has been continued here. Electro-optic switches are fast, reliable (no moving parts), bidirectional, rugged, and have wideband optical data transmission. They offer direct low-loss coupling to multimode fibers and the ability to integrate several waveguides and deflectors in one planar, monolithic substrate. Performance is achromatic over the visible and near-infrared range, and fabrication is carried out with conventional photolithographic liftoff techniques.

All crosspoints and matrices have been made from single-crystal plates of the ferroelectric material LiTaO_3 . The isomorphic material LiNbO_3 could also have been used, but LiNbO_3 is more susceptible to optical damage and has a higher birefringence; thus we prefer LiTaO_3 . Almost uniquely among commercial electro-optic materials, LiTaO_3 is available with the following combination of desirable properties: large sizes, freedom from domains-striae-imperfections, high resistivity, high purity, stability, and polishability. In small quantities, a 2.5 x 1.8 x .008 cm plate costs \$90 and a 6.0 x 1.0 x .008 cm plate \$250.

The LiTaO_3 starting material is undoped and uniformly poled. Plates are z-cut, with light propagating in the y-direction. The 75 μm plate thickness

is chosen to match the core diameter, 60 to 85 μm , of multimode fibers end-coupled to the plate. The Pockels linear electro-optic effect makes it possible to create waveguiding and switching structures within the crystal using electrodes on both large polished surfaces of the plate. (As distinct from the co-planar electrodes in single-mode optics, these are bi-planar.) The crystal is homogeneous in the absence of voltage, apart from a temporary passive effect (Sec. 4) stemming from metal overlays. With the voltage off, light in the crystal is free to spread out in the x-y plane, though it is strongly trapped in the z-direction due to lower-index dielectric cladding (e.g., optical cement) on the plate faces. The applied E-fields produce the desired x-y guiding. Those field are mainly along \vec{z} and are fairly uniform.

The crystal's refractive index in both the x and z directions is perturbed according to the relationships $\Delta n_x = \frac{1}{2}n_x^3 r_{13} E_z$ and $\Delta n_z = \frac{1}{2}n_z^3 r_{33} E_z$ where the electro-optic r-coefficients for clamped LiTaO_3 at $\lambda = 6328 \text{ \AA}$ are $r_{33} = 30.3 \times 10^{-12} \text{ m/V}$ and $r_{13} = 7.0 \times 10^{-12} \text{ m/V}$. Figure 1 shows the field dependence of Δn . Opposed top-and-bottom stripe electrodes permit one to set up "walls" or "barriers" in the crystal that are rectangular volumes, parallel to \vec{z} , at which the spatial distribution of refractive index decreases rapidly in step-like fashion.

Light will bounce off such barriers over a range of grazing-incidence angles; hence the reflection is multimode. One can make mirror-like objects or optical channels from parallel barriers (See Ref. 1 for a discussion of dipolar and quadripolar channels.) Both TE and TM light can be confined by total internal reflection at bounce angles that range from zero to the critical angle $\theta_c(\text{TE}) = \sqrt{2 \Delta n_x / n_x}$ or $\theta_c(\text{TM}) = \sqrt{2 \Delta n_z / n_z}$. The field-dependence of both critical angles is presented in Fig. 2. The TM light (polarized parallel to the dc electric field E_z) is more strongly confined, although the above square-root dependence makes the r_{13} coefficient 48% as effective for channeling TE light as r_{33} is for TM. While the switching potentials are time-varying, a steady bias voltage is required to induce and maintain the network of waveguides in the crystal.

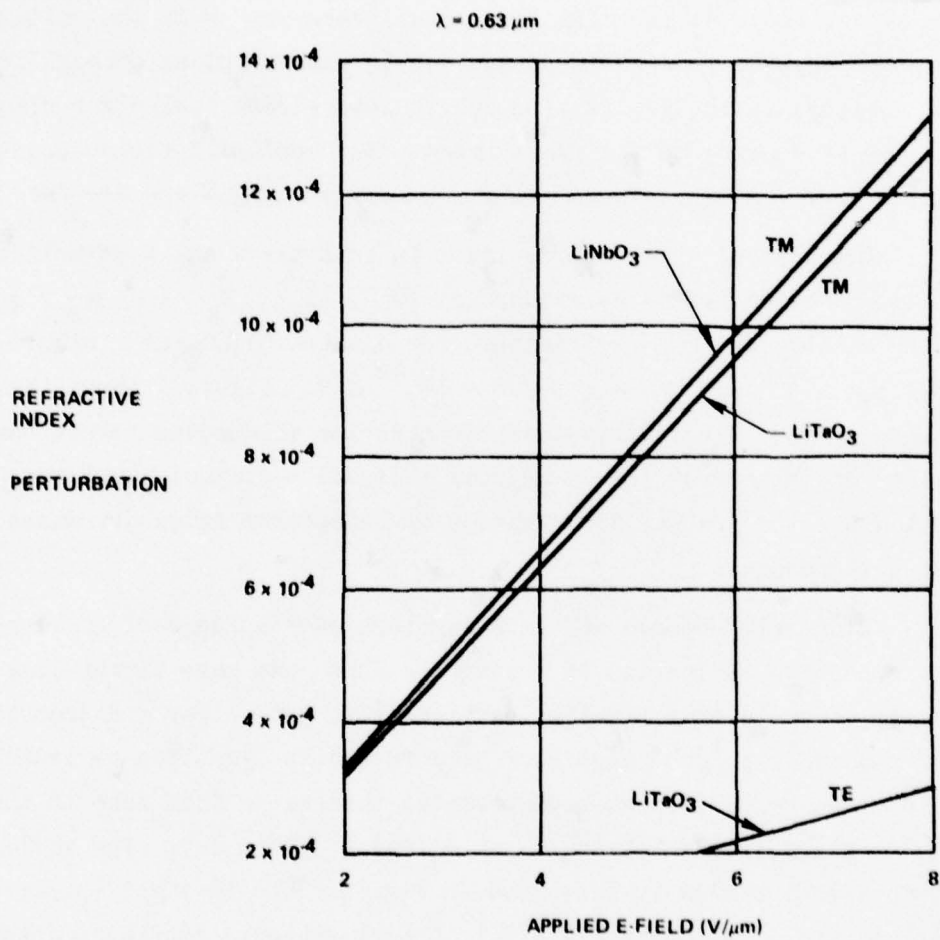


FIG. 1 Induced index perturbation in LiNbO_3 and LiTaO_3 as a function of applied field.

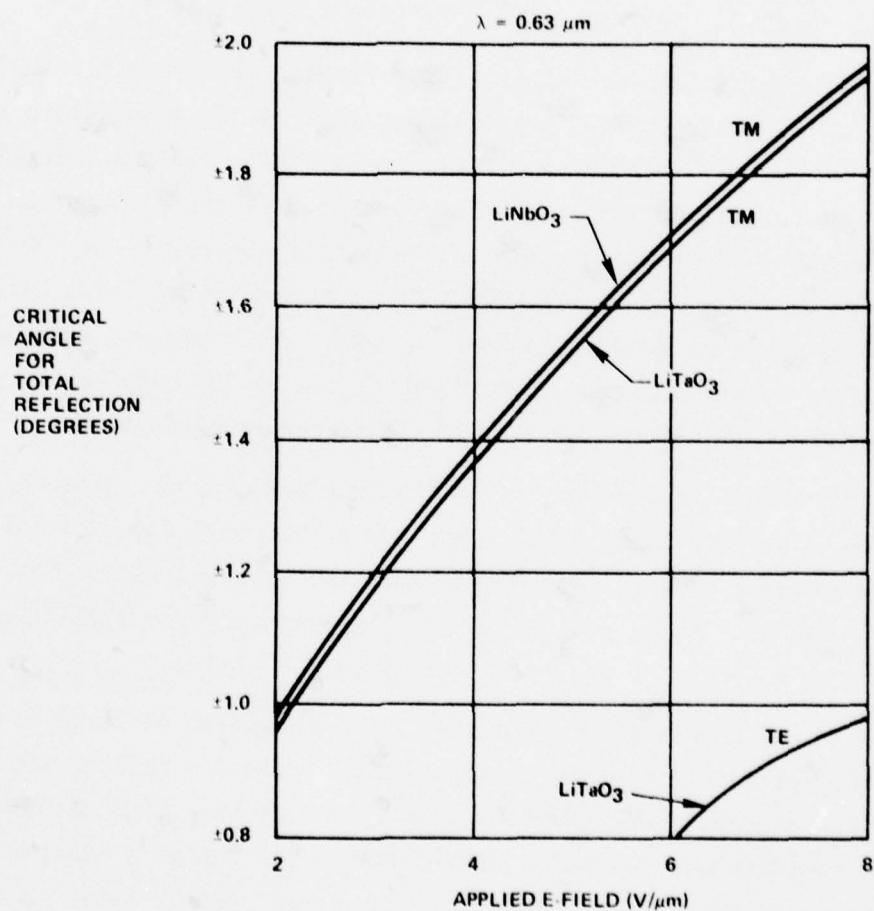


FIG. 2 Critical angle in LiNbO₃ and LiTaO₃ as a function of applied field.

3. THE OPTICAL MATRIX

A. Definitions

The matrix is an optical connecting network² that creates optical paths from its inputs to its outputs for a large number of possible connection patterns. The connection patterns or "configurations" are made in response to electrical commands (voltage pulses). The matrix is an assemblage of elemental switches known as optical crosspoints. These are four-port reversing switches that permute or do not permute signals between guides. The two crosspoint states are illustrated in Fig. 3. They can be described by terms such as "cross" or "bar", or "crossover" and "straight through".

If crosspoints are capable of switching all or nearly 100% of the input light to either output, those crosspoints can be joined into the so-called "permutation array", which is a compact, nonblocking² matrix. For N inputs and N outputs, only $\frac{1}{2}N(N-1)$ switches are needed to make the $N!$ possible connections. But if the crosspoints switch only a fraction of the light, say 50%, then the permutation array is not a good choice because the output level will vary dramatically from one matrix exit to the next. This happens because the number of bar-state crosspoints in a given optical connection path can vary greatly from one path to the next, depending on the configuration chosen.

Crosspoints developed here are four-port tapoff switches that switch 10 to 20% of the multimode light. The terms that best describe the multimode crosspoint states (Fig. 4) are "crossover" and "partial bar". The crossover state has low crosstalk, just as in the single-mode case, while the partial-bar condition is a hybrid or superposition of Fig. 3 states.

An appropriate and practical interconnection of these crosspoints is the square $N \times N$ matrix of N^2 crosspoints in which one half of the optical ports (the $2N$ unused ports) are terminated in optically absorbing material. We call this the "terminated crossbar". The crossbar for the $N=3$ example is shown in Fig. 5 together with the $N=3$ permutation array. Black lines in the diagrams represent optical waveguides. We show the guides crossing at a small angle, rather than 90° , because of the difficulties associated with deflecting multimode light through large angles.

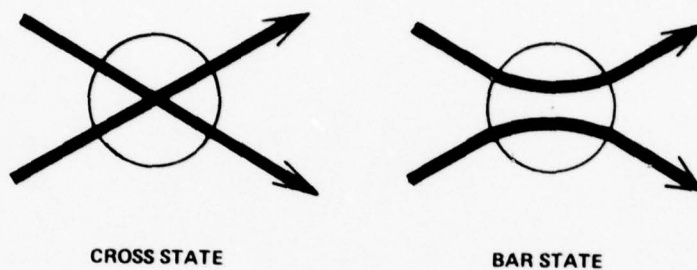


FIG. 3 Ideal states of crosspoint. Optical signals are, or are not, permuted between guides.

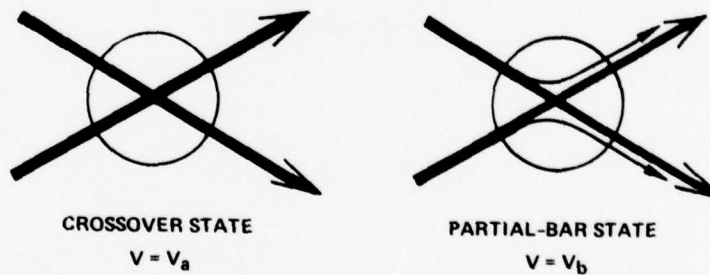


FIG. 4 Actual states of multimode crosspoint. Crossover state is near-ideal, but partial-bar state interchanges only a fraction of the light.

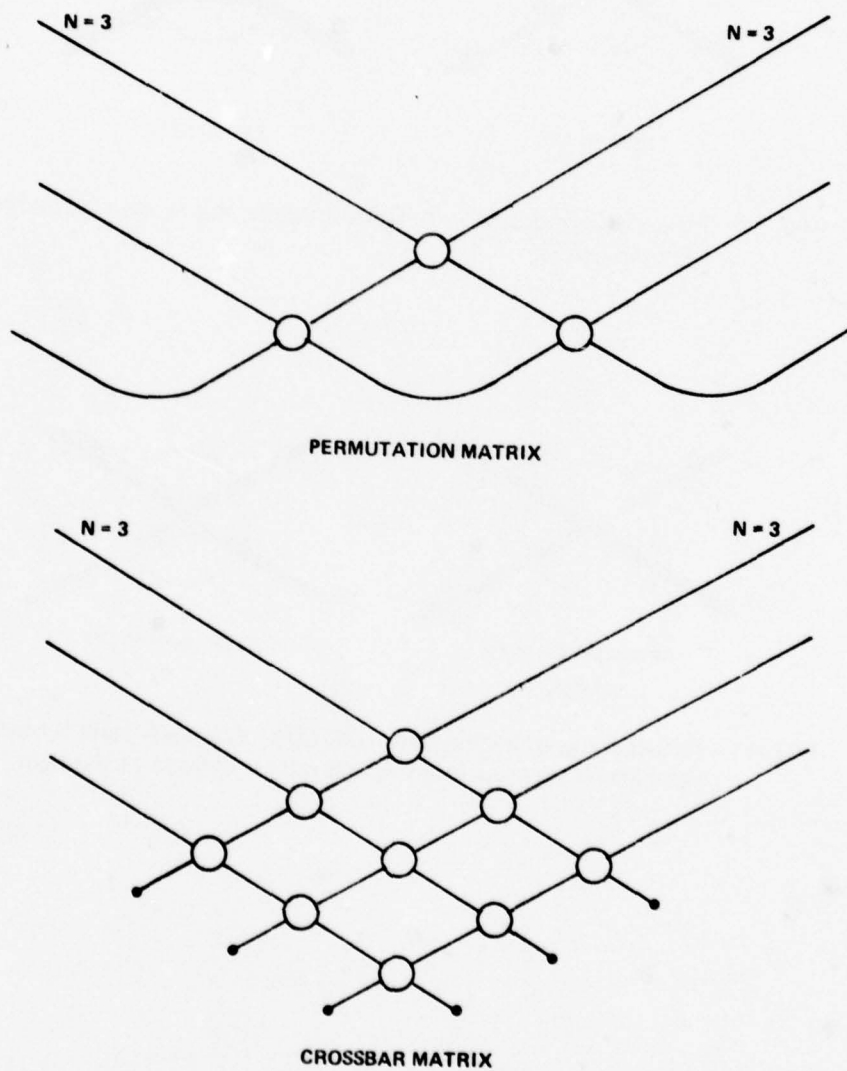


FIG. 5 Topology of permutation matrix and crossbar matrix. Circles represent crosspoints, black lines denote optical guides, and dots are absorbers.

Supplementing the square array, one can just as easily fashion a "rectangular matrix" which is an $N \times M$ crossbar array of switches, for example, the $N > M$ "concentration network" of Fig. 6(a), which is useful for time-division multiplexing. If desired, one can also make a one-sided connection network² such as the triangular matrix of Fig. 6(b). Here, the absorbing terminations have been replaced with optical mirrors, all located on one surface of the crystal.

B. Addressing

To achieve simultaneous N -fold pairing of inputs with outputs, only one crosspoint in each row of the matrix (and only one in each column) is put into the partial-bar state at a given instant. We say that light "turns a corner" only once in the matrix. Although an optical signal passes through several crossover-state crosspoints, those devices have low loss and the signal strength is virtually unchanged from one path to the next. Hence, because only one crosspoint per path is "turned on", the optical signal power at any matrix output is the same, regardless of matrix configuration. This would not be true in the permutation case.

C. Configurations

There are $N!$ possible configurations for the $N \times N$ crossbar. Since the goal of this contract is a 3×3 system, we illustrate in Fig. 7 the six configurations of the $N = 3$ matrix. Crosspoints put into the partial-bar state are shown by dark circles, the remainder being in crossover states.

D. Duplexing

Two-way communication, although not an explicit goal of the 3×3 system on this contract, is a desirable feature for the switched fiber network joining optical terminals. The present system has been made unidirectional for simplicity, but the electro-optic matrices are intrinsically bi-directional (because of their symmetry and because of optical reciprocity).

For completeness, we shall describe three methods of obtaining bi-directional switching. These are shown in the system diagrams of Fig. 8. The simplest technique is to replicate the matrices, one for each direction; Fig. 8(c). Another duplex approach uses the matrix reciprocity and employs Y-couplers in front of each terminal, Fig. 8(b). The third method, half-duplex,

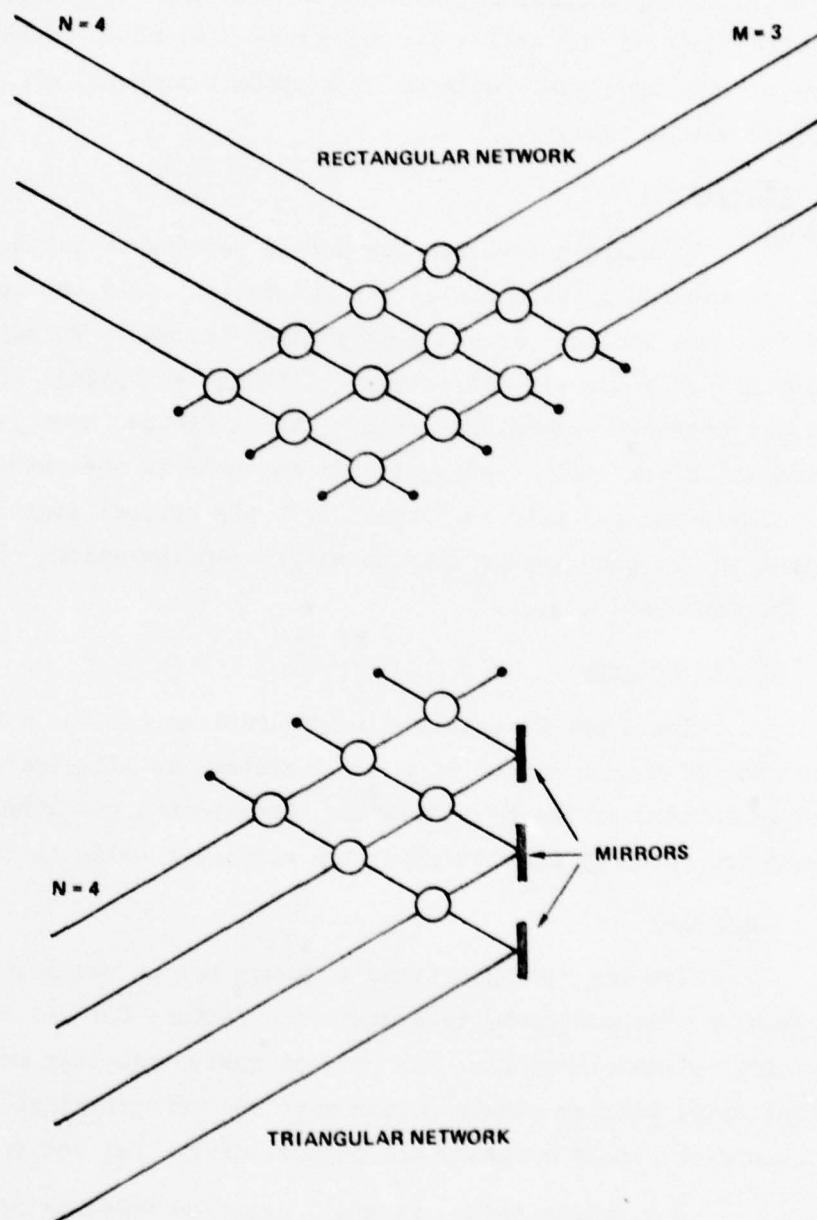


FIG. 6 Topology of rectangular matrix and one-sided matrix.

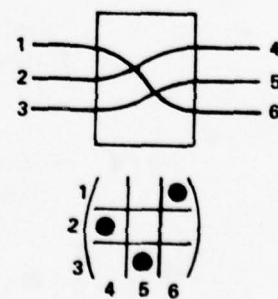
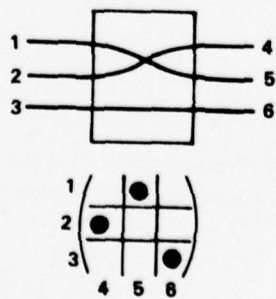
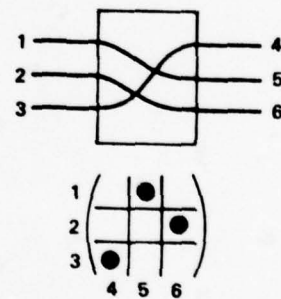
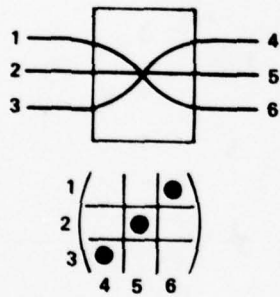
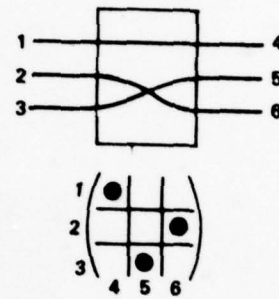
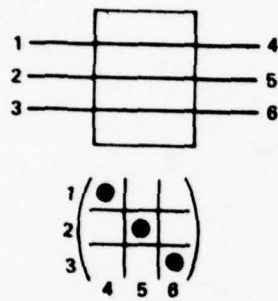


FIG. 7 Six possible configurations of 3 X 3 optical matrix. Electrical addressing of crosspoints is shown.

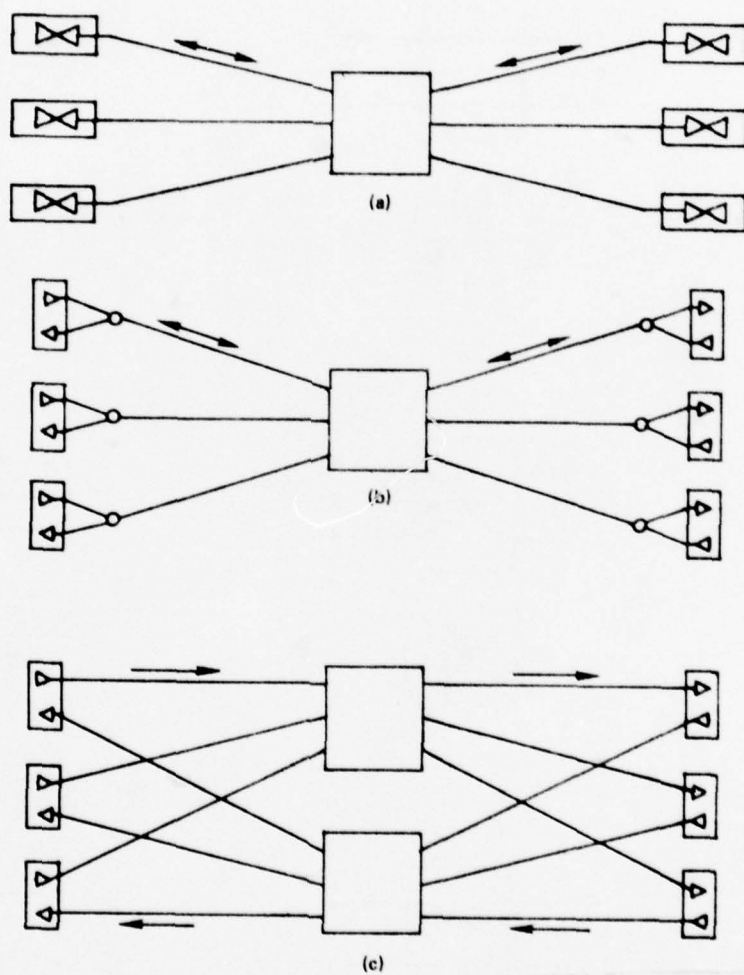


FIG. 8 Duplex communication in matrix-switched network, using (a) combination source/detectors, (b) fiber-optic Y-couplers, and (c) two matrices.

makes use of the half-duplex either/or property of certain GaAs detector/emitter devices; Fig. 8(a).

E. Optical Crosstalk Theory

We discussed in Ref. 3 the signal-to-crosstalk ratios at the output ports of the $N \times N$ crossbar and compared the results to those for an individual switch. Considering the minimum S/C ratio, we found that the optical crosstalk in the N^2 array is, in theory, a factor of $(N-1)$ larger than that of the crosspoint. For example, the 3×3 matrix should have 3 dB more crosstalk than one of its switches alone.

F. Fiber Coupling

Fiber light is strongly trapped in the z-direction and free to spread in the x-y plane of the matrix crystal. When entering the crystal normally, the fiber light cone angle is reduced by the factor n_f/n_c where n_f is the fiber core index and n_c the crystal index. However, the cone angle will still be relatively wide.

Considering fringing-field overlap in our electro-optic channels, we find that an optical x-y cone of $\pm 1.5^\circ$ can be trapped at maximum voltage, but that the light confinement and switching efficiency drops off rapidly at ray-angles above 1.5° . Therefore, we need a means for reducing the high-angle-ray content of fiber light in the matrix.

Nelson and McMahon of our laboratory have proposed and tested a means for one-dimensional collimation of light at the fiber/crystal interface. This technique is to use off-normal incidence of fibers on the crystal in the x-y plane (in a direct, butt coupling arrangement), and to let the Snell's-law refraction give the desired "bunching" of light rays. Specifically, the demagnification or collimation factor (m) at the interface is given by the relations

$$n_f \cos \theta_f = n_c \cos \theta_c \quad (1)$$

$$\theta_f^2 = (n_f^2 - n_c^2) / (n_f^2 - m^2 n_c^2) \quad (2)$$

where θ_f and θ_c are the ray angles (measured with respect to the interface normal) in the fiber and crystalline media, respectively.

With this oblique incidence, one needs a wider channel to accept light over the fiber cross-section, and a de-collimation should be done at the matrix outputs so the output fibers can capture all the channeled light. The fiber ends and both matrix ends are cut obliquely and are coupled together as illustrated in Fig. 9 (a view looking down at the x-y plane) which indicates the ray angles in both media.

A specific calculation will be made for our experiment in which the LiTaO_3 matrix has a nearly isotropic index of $n_c = 2.18$ at $\lambda = 0.63 \mu\text{m}$ and the silica fiber has $n_f = 1.47$ at the same wavelength. We now compute, from Eqs. (1) and (2), the fiber and matrix incidence angles as a function of the optical collimation factor, the result being shown in Fig. 10. An 0.5° correction is needed to θ_c as shown in the graph, because the light-distribution is not symmetrical over the channel cross-section.

What collimation factor is needed for an input numerical aperture of 0.15 in air? This fiber would launch a $\pm 3.9^\circ$ cone without collimation, so a collimation factor of $3.9/1.5$, or 2.6 is required in our system.

G. Optical Insertion-Loss Theory

We shall now calculate the optical loss of the addressed matrix, taking into account various contributions, and making some assumptions about switching efficiency and mode-launching conditions. In doing this, we will follow the approach of Nelson (Ref. 4, pp. 17-18). First, we assume that the fiber launches equal amounts of TE and TM modes in the angle-terminated crystal. Although the TE or TM reflection losses are only 0.66 dB at normal incidence, these Fresnel losses go up at a 2.6-fold collimation factor to 1.0 and 4.5 dB, respectively, and, when an anti-reflection fluid is added, the TE and TM losses at both in + out interfaces become 0.5 and 2.5 dB, respectively. Also, since $r_{13} \approx 0.25 r_{33}$, about 50% of the TE light is not guided, assuming 100% trapping of TM.

Crosspoint switching efficiency is, somewhat optimistically, taken as 30% for TM modes (-5.2 dB) and 15% for TE (-8.2 dB) at full voltage. In our addressing method, light traverses at most $2N-2$ crossover crosspoints. Taking this crosspoint propagation loss to be 0.3 dB/cm, we assign a value of 1.5 dB to the matrix propagation loss for $N = 3$.

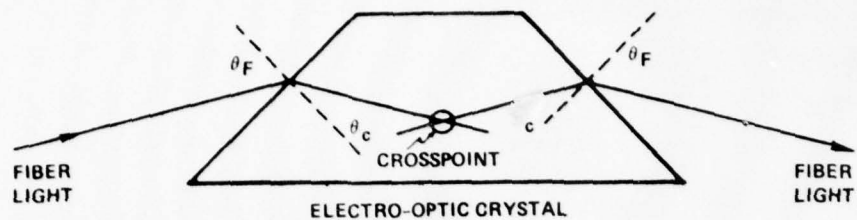


FIG. 9 Coupling of input and output fibers at off-normal incidence to crystalline matrix.

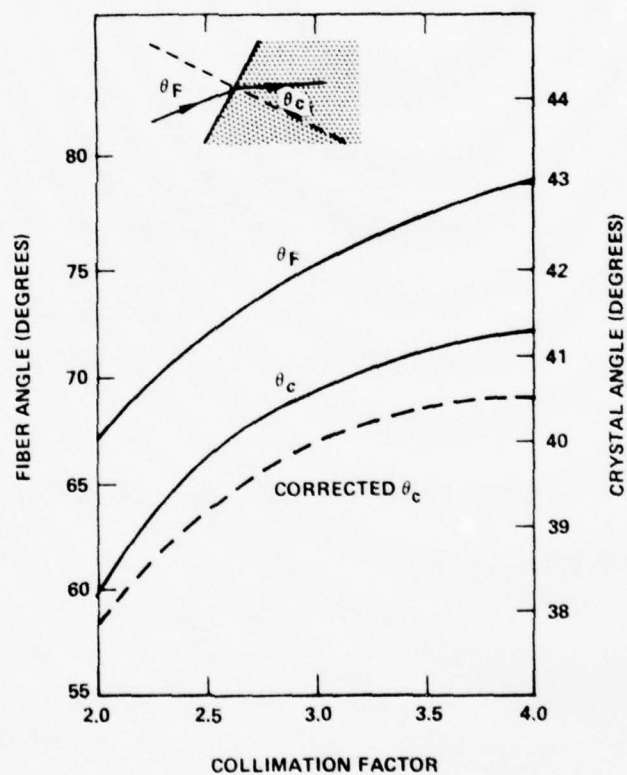


FIG. 10 Theoretical dependence of fiber and crystal end-fire-coupling angles upon optical collimation factor.

Loss also arises from "size mismatches". Since the fiber and crystal will differ slightly in height and, since the channel cross-section is quasi-rectangular, there will be approximately a 1.5 dB mismatch loss between an 85- μm -diam fiber core and a 75- μm -high channel. Also, the channels are not "sharp" in practice because fringing E-fields spread laterally beyond the nominal 9-mil width; thus, light initially picked up will spread to a wider region and not be completely recaptured by the output fiber, leading to an estimated 1 dB loss.

Table 1 lists the various insertion-loss contributions. Adding them up for both polarizations and taking the average, we find that the switched 3 x 3 array has a theoretical throughput loss of about 14 dB.

H. Fiber-Optic Intercom System

According to the contract Statement of Work, we intend to build a multi-terminal system linked by monofibers like that shown in Fig. 11. The matrix acts as an "optical switchboard" between the two groups of subscribers". In designing the specific system, we made a number of choices such as a 9-element manual keyboard for control; 0.1, 0.2 and 0.4 Mbps internally generated optical data; angle terminations to matrix; oscilloscope display of received information; optical sources grouped in one box for convenience; receivers similarly grouped; and connectors on the input fiber to allow replacement of LEDs if desired. A system diagram for the actual hardware delivered to RADC/ET is presented in Fig. 12.

4. THE CROSSPOINTS

A. Design and Results

The compound crosspoints originally developed¹ had an optical cross-talk level of -25 dB, but that was obtained at the expense of a 6-cm device length. We then developed a "simple" crosspoint that had the virtue of being much more compact, about 1 cm long. As illustrated in Fig. 13, it consists of a single power-division element situated at the intersection of two electro-optic channels.¹ In terms of the crosspoint length L_c , a crossbar matrix has a minimum length of $(2N-1)L_c$, which is $5L_c$ for our $N = 3$ goal. Hence, because

	<u>TE</u>	<u>TM</u>
Reflections (with AR fluid)	0.5	2.5
Fringing field	1.0	1.0
Unconfined TE light	3.0	---
Size mismatch	1.5	1.5
Switching loss of tapoff-state crosspoint	8.2	5.2
Switching loss of 2N-2 crossover crosspoints	<u>1.5</u>	<u>1.5</u>
	15.7	11.7

average = 13.7

Table 1. Theoretical loss components in dB for addressed 3 x 3 matrix. Fiber-coupled matrix is angle-terminated.

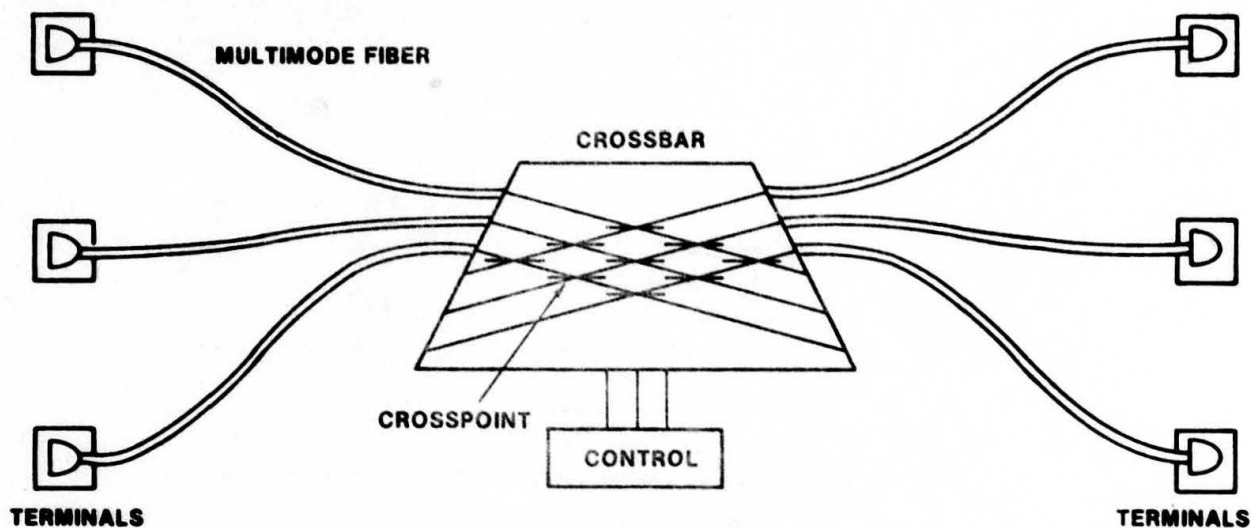


FIG. 11 General system diagram for switched fiber-optic intercom.

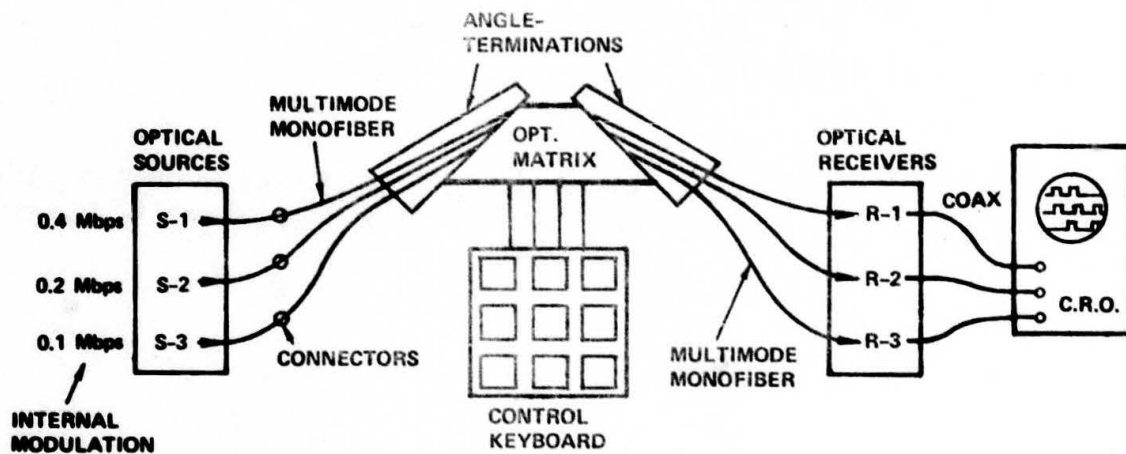


FIG. 12 Specific features of the six-terminal crossbar-switched system delivered to RADC/ET.

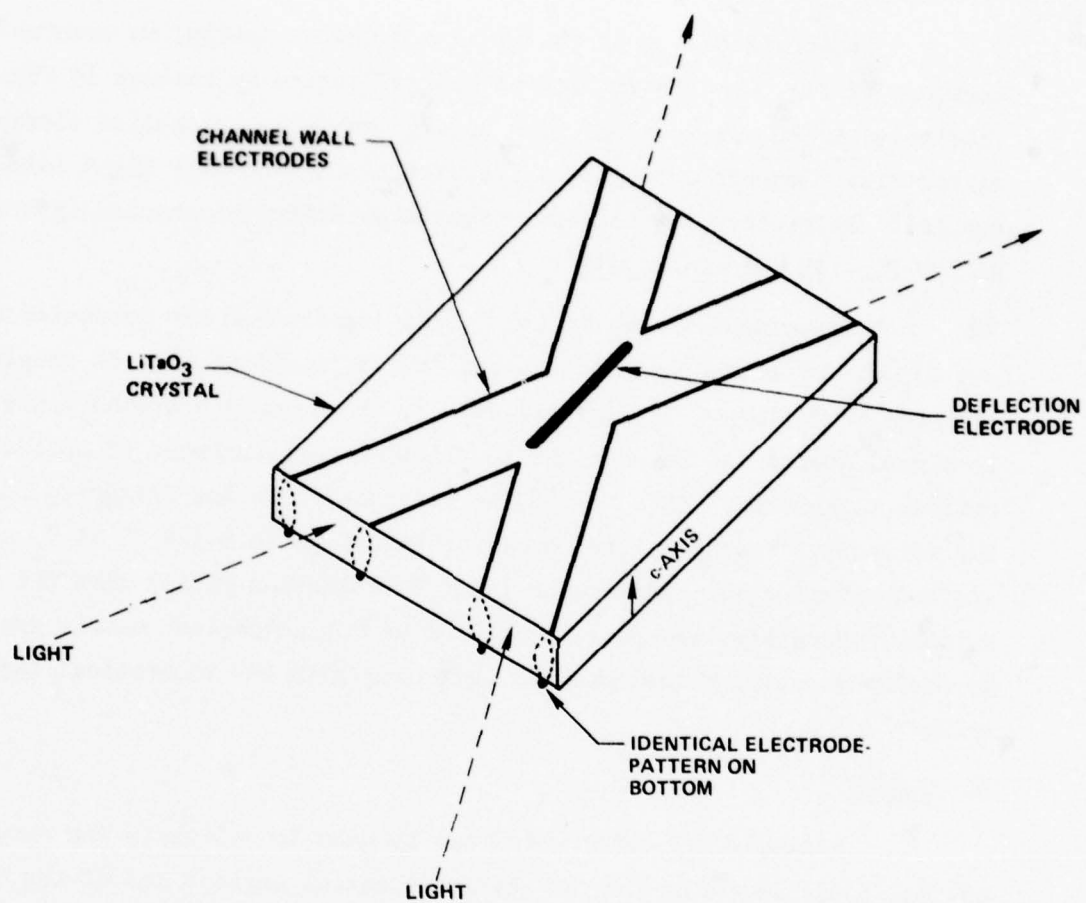


FIG. 13 Layout of four-port reflective crosspoint device.

high-quality 7-cm LiTaO_3 plates are available, the 1 cm crosspoints are acceptable for 3 x 3 matrixing.

Before deciding on the final crosspoint design, we examined two versions of Fig. 13 — the refractive and reflective approaches of Fig. 14. We fabricated LiTaO_3 devices in which an electro-optic prism-like element (or mirror-like element) deflected a fraction of the incoming light into the cross-channel. Refractive devices that have three different channel intersection angles as per Fig. 15 were fabricated.

Experimental results for refractive devices are presented in Figs. 16 and 17 and may be compared to the reflective result of Fig. 18 obtained under the same conditions. In Figs. 16 and 17, the channel crossing angle $\phi = 3.5^\circ$ is a good compromise between the conflicting ϕ -dependences of optical tapoff and optical background. At $\phi = 3.5^\circ$, we concluded from the foregoing results that the reflective crosspoint had a higher tapoff ratio (-5.4 dB at $V_b = 500$ V dc) and better crosstalk performance (-20 dB extinction ratio) than the refractor-switch. Therefore, we chose the reflector for subsequent matrix experiments. We shall now compare the observed switching with the theoretical tapoff developed below.

B. Theory

A simple ray-optic model can be used to calculate the amount of switched optical power as a function of the intersection angle ϕ and of the numerical aperture of input light. Figure 19 shows a top view of the reflective crosspoint, defining the "pencil" of rays coming in on-axis to the channel within a $\pm\theta$ cone. Since we assume that the waveguide walls and reflector boundaries are "sharp" (no fringing) and that the angular distribution of light is square rather than gaussian, the model is admittedly simple; nevertheless, it does suggest the general trend of events.

Looking at Fig. 19, we define α as the incidence angle on the partial-mirror with respect to the input axis, and β as the incidence angle with respect to the mirror plane. The electro-optic deflection angle γ is measured with respect to the input axis and, by hypothesis, the active reflector is oriented symmetrically, at exactly half the channel-intersection angle ($\phi/2$). We further

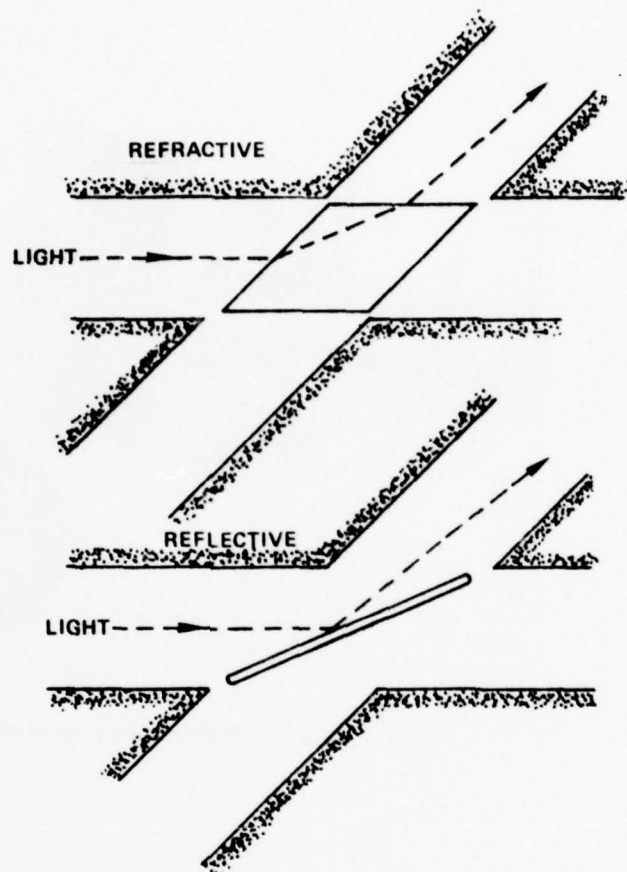


FIG. 14 Two methods of deflecting light in a crossbar.

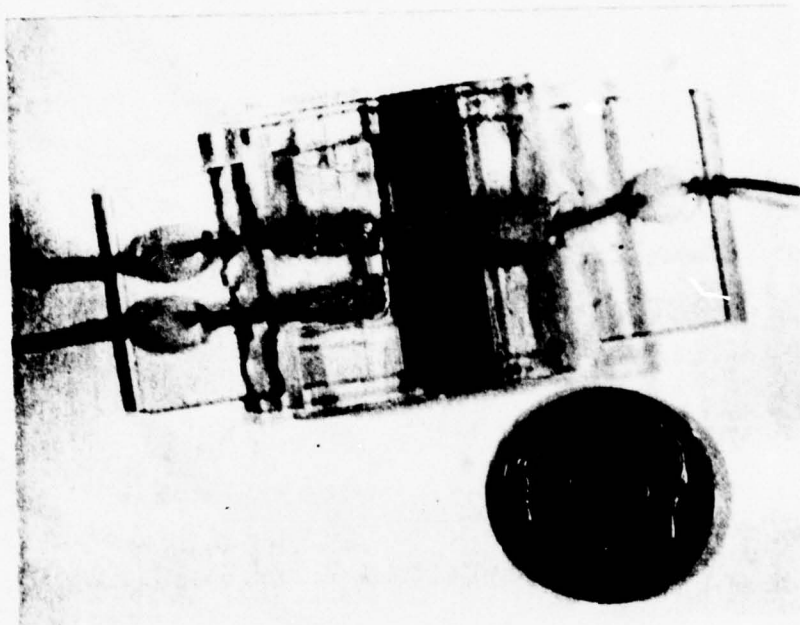


FIG. 15 Refractive crosspoint device.

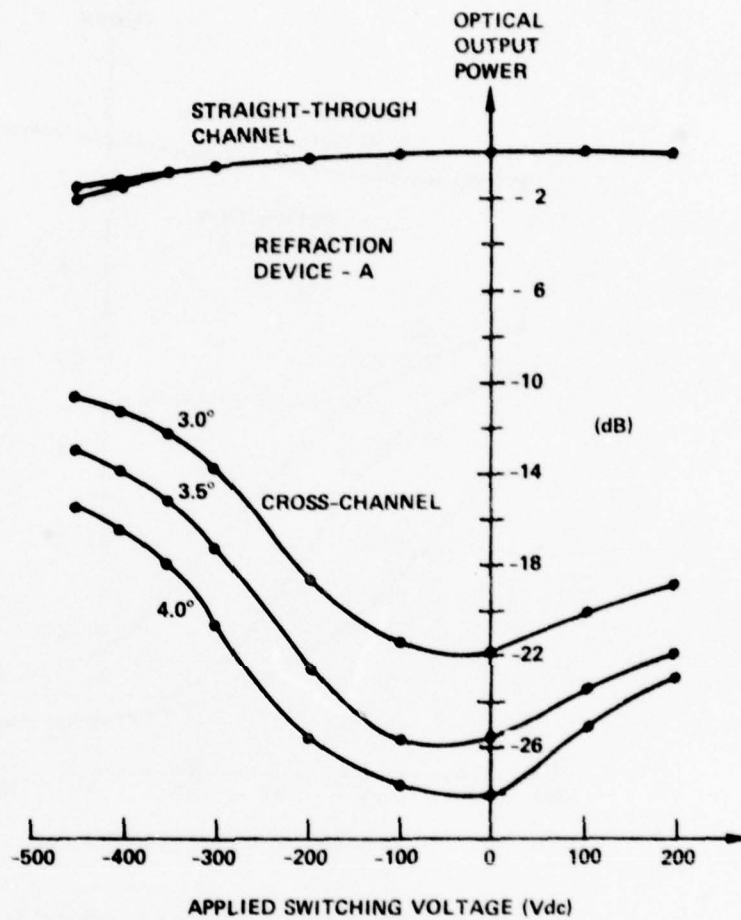


FIG. 16 Observed performance of refraction crosspoint A.

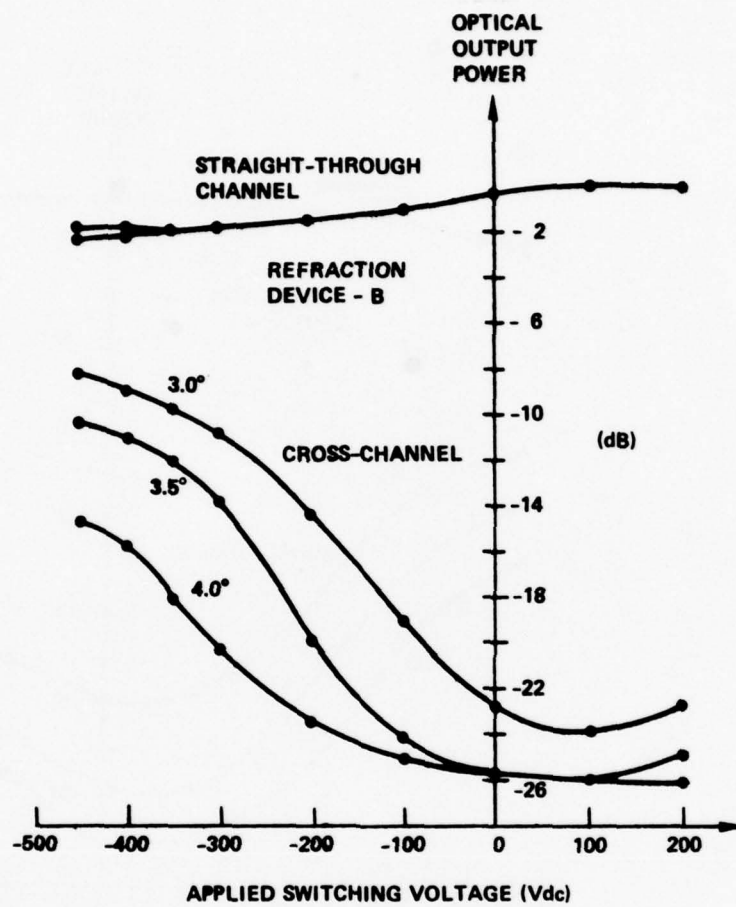


FIG. 17 Observed performance of refraction crosspoint B.

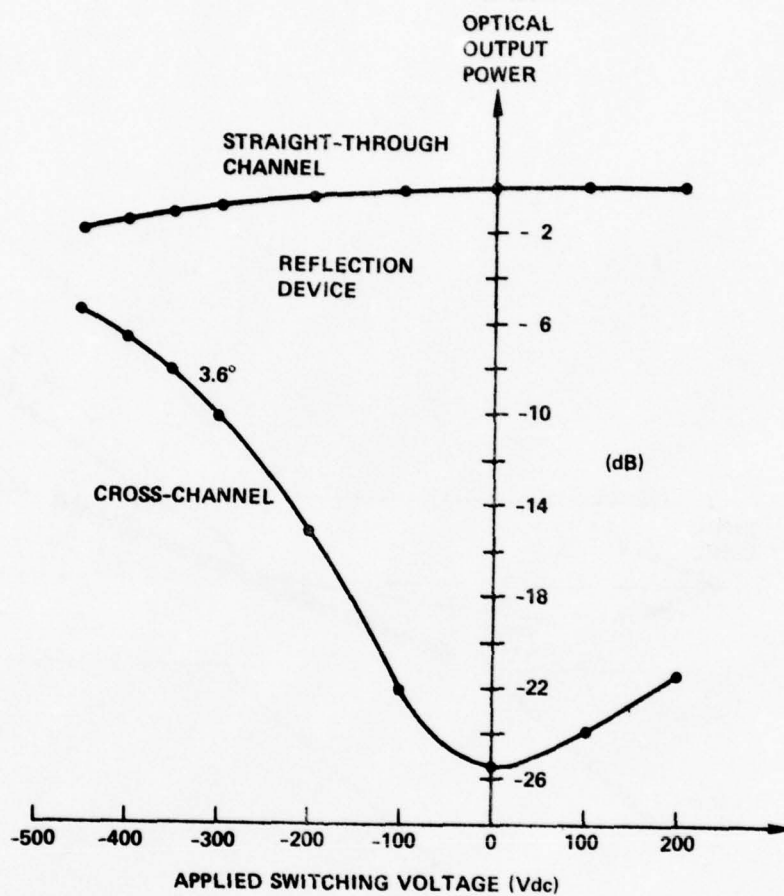


FIG. 18 Observed performance of reflection crosspoint.

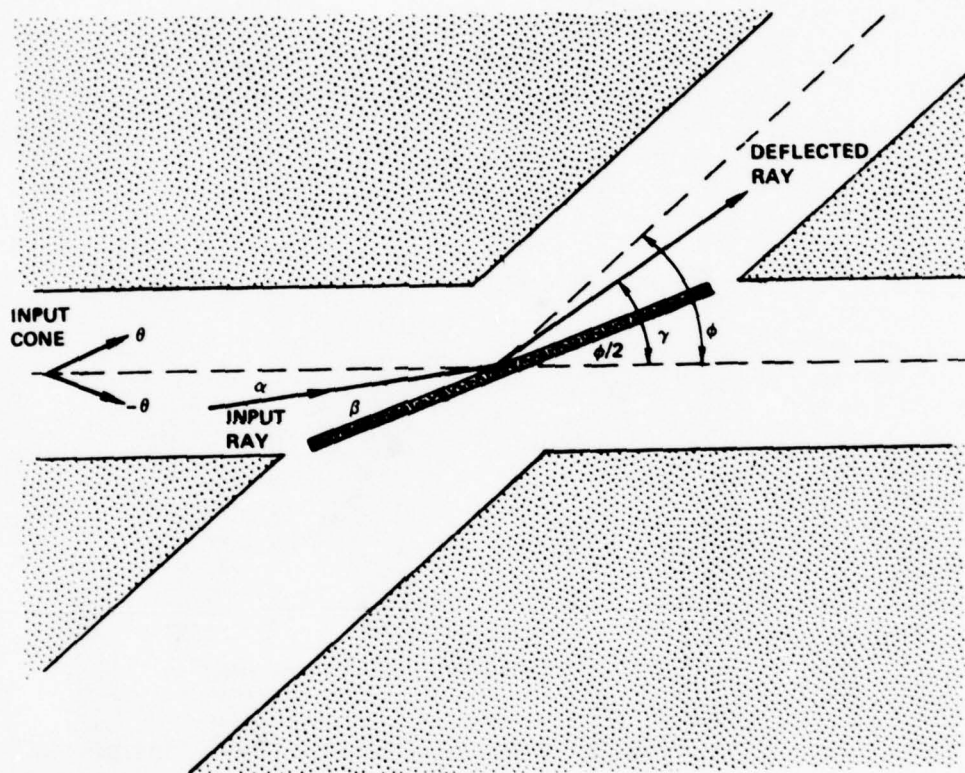


FIG. 19 Top view of reflection crosspoint that defines angles of switched light rays, incident rays, and channel intersection.

assume for simplicity that the switching voltage V_b is the same as the waveguide voltage V_w , which implies that critical angle θ_c will be the same for mirror and walls. Also, for convenience we assume only TM modes are present and that θ_c is the TM trapping angle. By hypothesis, $\theta < \theta_c$.

The intersection angle is chosen to be more than twice the critical angle $\phi > 2\theta_c$ in order to "totally isolate" the crosschannel from the incidence channel when $V = V_a$. Optical deflection occurs for $0 \leq \beta \leq \theta_c$ and transmission for $\beta > \theta_c$. The deflection angle is $\gamma = \phi - \alpha$ and the crossguide accepts rays $\phi - \theta_c < \gamma < \phi + \theta_c$. Thus, all deflected rays are accepted because $\phi > 2\theta_c$. Assuming all the crossguided light is captured at the switch output-end, we now compute the switched power by finding the range of input angles $\alpha_1 < \alpha < \alpha_2$ that is affected.

Noting that $\alpha + \beta = \phi/2$ and using the limiting values $\beta = 0$ and $\beta = \theta_c$, we find that the maximum- α deflected ray is $\alpha_2 = \frac{\phi}{2} - \theta_c$ and the minimum- α deflected ray is $\alpha_1 = \theta$ since $\theta < \theta_c < \frac{\phi}{2}$. The fraction of input light that is switched is $(\alpha_2 - \alpha_1)/2\theta$ and, substituting the foregoing α -results, we find that the fraction deflected is $[\theta - (\phi/2 - \theta_c)]/2\theta$. For convenience, we want to express this in terms of the normalized numerical aperture θ/θ_c and of the normalized channel crossing angle ϕ/θ_c . In so doing, we obtain the result

$$\text{Fraction deflected} = \frac{1}{2} \left[1 + \frac{1}{(\theta/\theta_c)} - \frac{\phi/\theta_c}{2(\theta/\theta_c)} \right] \quad (3)$$

With the aid of Eq. (3), we have plotted in Fig. 20 the predicted output power of the crosspoint switch (on a dB scale relative to the input power) as a function of the input numerical aperture. Corresponding to experiments, the input light cone ranges from 40 to 100% of θ_c in the figure, and practical values of intersection angle, from 2.2 to 2.6 times θ_c , have been taken as a parameter in the graphs. For large numerical apertures, -5 to -4 dB switching is predicted. Somewhat surprisingly, a higher switched power is predicted for a wide on-axis light cone than for a narrow cone.

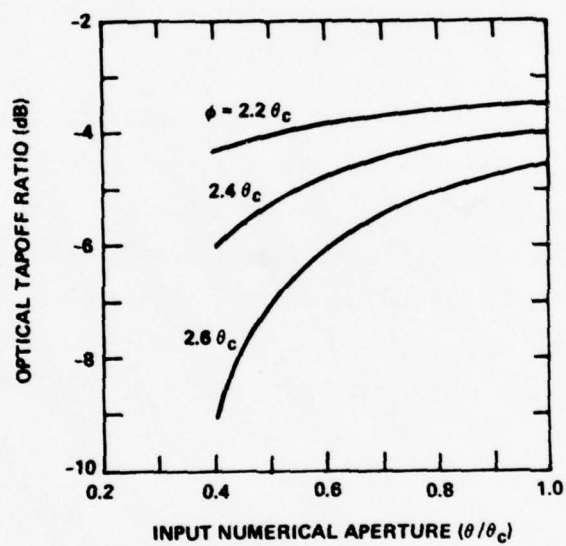


FIG. 20 Calculated values of switched optical power for Fig. 13 crosspoint as a function of input light cone angle. Intersection angle is taken as a parameter.

C. Comparison

Experimentally, we had $\theta/\theta_c \approx 1$ because the 0.07-NA-light filled the electro-optic guide, and $\phi \approx 2.4 \theta_c$ because the effective TM trapping angle was 1.5° due to field-overlap in the quadripolar guide. Therefore, from Fig. 20, a switching ratio of -4.1 dB is predicted. The observed -5.4 dB optical tapoff is in reasonably good agreement with this. When decreasing the numerical aperture by 50% it is difficult to confirm experimentally the predicted 1-dB decrease in tapoff because this change is within experimental uncertainties; for example, one finds tapoff variations in practice because the ratio is sensitive to errors in axial alignment of the input light beam. (The theoretical and experimental switching ratios cited here do not include the various input/output coupling losses to the crystal.)

D. Passive Effect

As discussed previously^{1,2} our electro-optic devices have a passive effect, temporary in nature, that enables light to be guided without voltage applied. Since the effect fades out completely in several days, it does not impair device reproducibility or device function.

When metal is deposited on the LiTaO_3 surface and when the crystal is heated into the 70 to 150°C range, the refractive index of the crystal decreases (never increases) in bulk regions directly under the metal. Initially, the index shift is about 10^{-3} , subsequently fading to about 10^{-5} after two weeks. Whether ionic or electronic motion (indiffusion, out-diffusion, etc.) is responsible for this, we are not certain.

Measurements reported here were made after the effect became insignificant.

5. THE 2 x 2 MATRIX SWITCH

A. Design

Our first matrix, the multimode 2 x 2 crossbar, contained four reflection-type crosspoints. The matrix consists of two pairs of straight parallel electro-optic channels that intersect at a shallow angle in the LiTaO_3

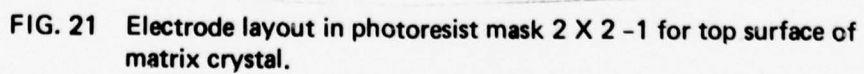
plate. Of the four waveguide ports at each end of the matrix, only half are used: two inputs and two outputs. At the remaining ports, light is neither injected nor collected.

The matrix design retained the 9-mil channel width, 3.6° crossover angle, and 1-mil reflector width of the crosspoints. A channel separation of 27 mils center-to-center was felt to give good interchannel isolation while keeping the matrix small. Small metal bridges are placed across the optical channels at 90° to the propagation direction (which does not affect the guided light) in order to join equipotential portions of the top-surface electrode pattern. Those areas can then be accessed with one contact.

The resulting electrode patterns for the large surfaces of the polished LiTaO_3 plate are shown in Figs. 21 and 22 (masks 2x2-1 and 2x2-2) with details of the switching regions shown in Figs. 23 and 24. These crossbar matrix patterns are registered directly across from one another on the plane-parallel crystal faces. The complicated pattern 2x2-2 is actually a continuous film of metal set at ground potential (the common electrode). Pattern 2x2-1 consists of "walls" for channels and four "bars". The 1-mil-wide crosspoint bars are independently actuated optical power dividers, 0.76 cm long. The matrix interaction length is 2.92 cm, not counting lead-in waveguides.

It became evident that there was a problem of gaining electrical access to the bars. The wall pattern could have been interrupted in four places where conductive paths from bars would have fanned out to both sides of the crystal. But this would have cut the channel wall pattern into about a dozen pieces, some of which would have been inaccessible.

We therefore made contact to the top of each bar. The gold 2x2-1 pattern was covered with a very thick insulating layer of photoresist; narrow openings, precisely over the bars, were made by exposure and development. Then, conductive metal paths were deposited atop the resist. They went over the channel walls (electrical crossovers) and down into the 0.9-mil x 100-mil holes where they touched the bars. The resist thickness was 60 to 70 μm to stand off 450 V dc between waveguides and crosspoints. Figures 25 and 26 show the masks employed to make contact to crosspoints and to the 2x2-1 channel walls. Mask 2x2-3 is an arrangement of windows created in the insulating layer, and mask 2x2-4 delineates



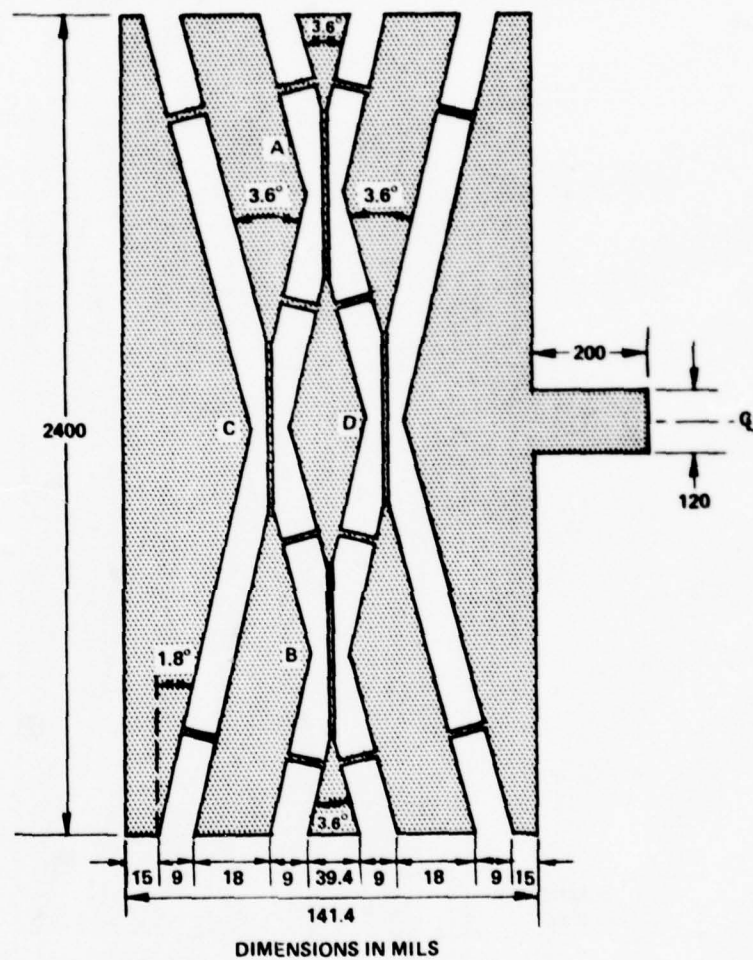


FIG. 22 Electrode layout in photoresist mask 2 X 2 -2 for bottom surface of matrix crystal.

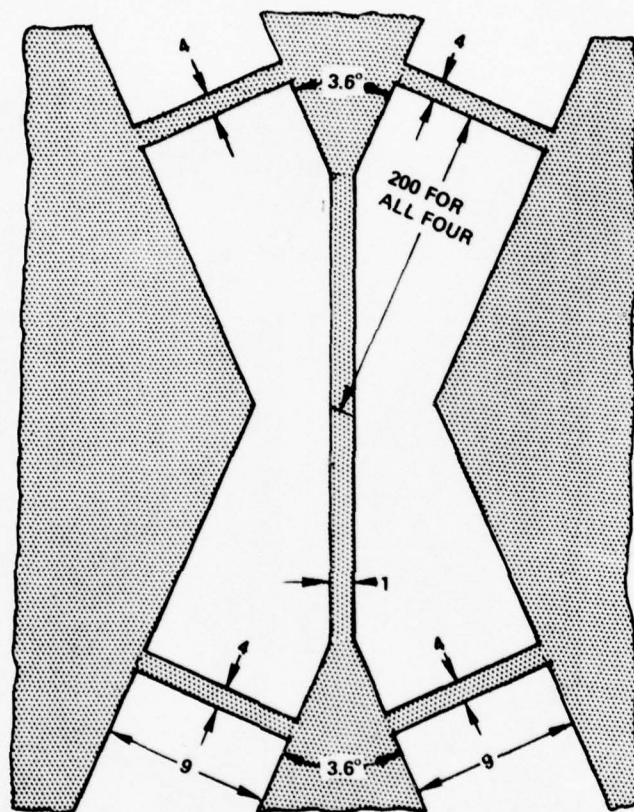


FIG. 24 Detail of crosspoint region in Fig. 22 ground plane.

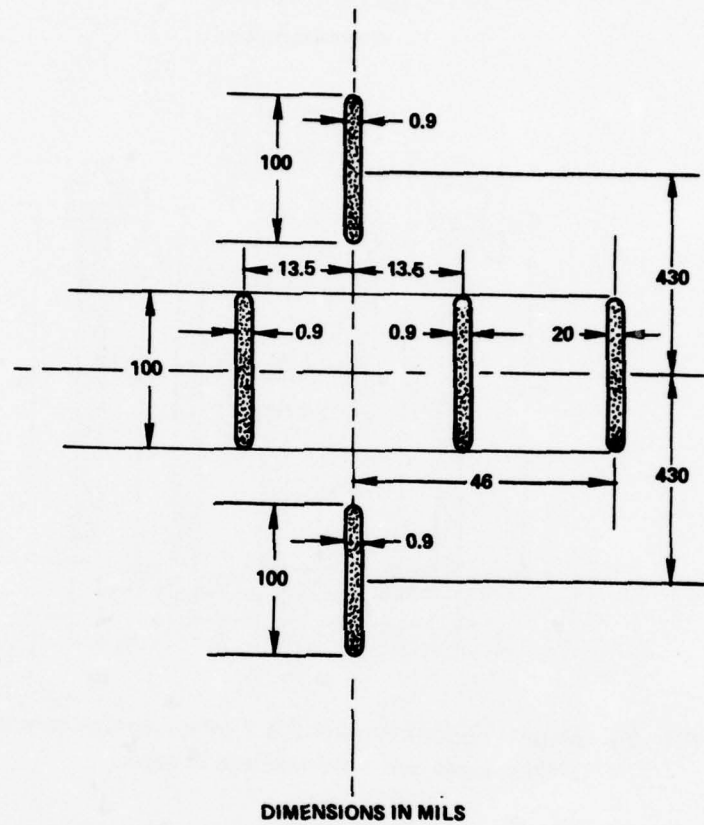


FIG. 25 Photoresist window-mask 2 X 2-3 for making electrical contact to crosspoints and channel boundaries.

METAL EVAPORATION MASK
DIMENSIONS IN MILS

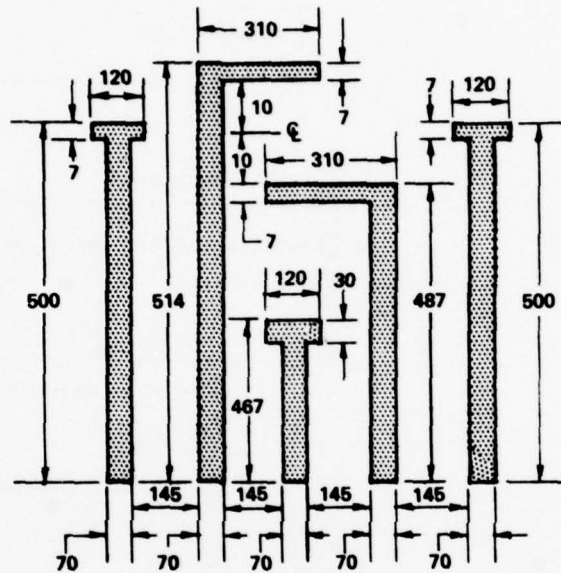


FIG. 26 Metal evaporation mask 2 X 2 -4 for making conductive fan-outs.
Shaded areas represent openings in mask.

the metal paths that go from one side of the crystal to the aforementioned windows in the crystal's midregion. Further details of the device fabrication process are given in Appendix A.

B. Results

A fully operational matrix was built in a 4.3 cm x 1.0 cm x 0.0087 cm LiTaO_3 crystal. Figure 27 is a photograph of the completed 2 x 2 matrix. This is the first multimode optical switch of its kind reported in the literature. A close-up view of the switching region is provided in Fig. 28. The matrix ends (Fig. 27) have been cut at right angles for normal-incidence laser coupling.

Focused 0.63- μm laser beams, polarized parallel to the crystal z-axis, were injected on-axis into the matrix and, by choosing the appropriate lens, the input numerical aperture was restricted to 0.07. Using our 2-out-of-4 addressing technique, we applied $V_a = -20$ V dc (which helps inhibit crosstalk) to unselected crosspoints, and measured the switched optical power (matrix throughput in cross-channels) as a function of the crosspoint addressing voltage V_b , from $V_b = -100$ to $+600$ V dc. The waveguide voltage was held at $+420$ V dc to keep the crossover voltage $V_w - V_a$ below 450 V dc. The experimental results are presented in Fig. 29.

We found the optical crosstalk between adjacent matrix outputs, as per Fig. 29, to be -16 dB. The internally switched optical power in the matrix was approximately -8 dB at 550 V dc. Adding to this the 1.5 dB input-plus-output coupling loss of the matrix and the approx 1.5 dB propagation loss of the unaddressed crossover crosspoints, the optical insertion loss of the addressed matrix is approximately 11 dB as seen in the figure. When the input/output NA was decreased to 0.03, the magnitude of the switched optical power did not change significantly (nor did the insertion loss), but the optical extinction ratio improved to 20 dB.

6. DESIGN OF 3 x 3 MATRIX SWITCH

We made the 3 x 3 array a straightforward extension of the 2 x 2 array because the latter had adequate performance. There are now nine independent deflectors (crosspoints) and two trios of intersecting channels, of which three input ports and three output ports are used. The 3 x 3 photomasks include

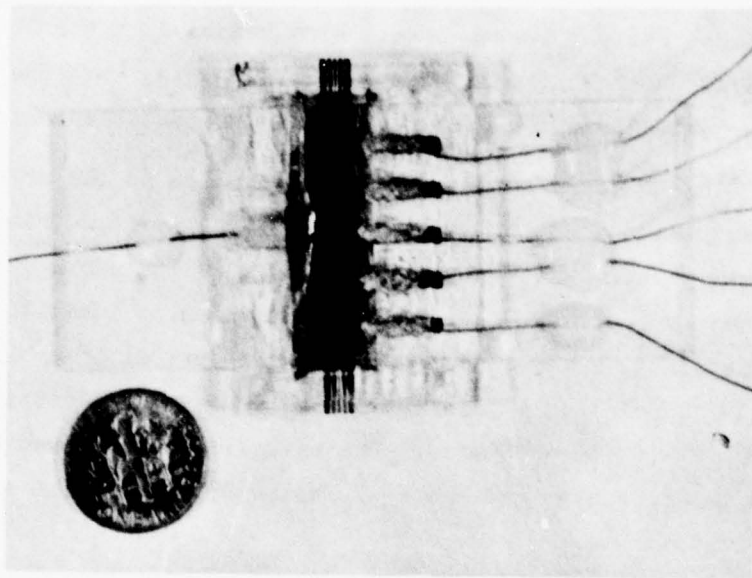


FIG. 27 Experimental model of multimode 2 X 2 optical crossbar matrix.

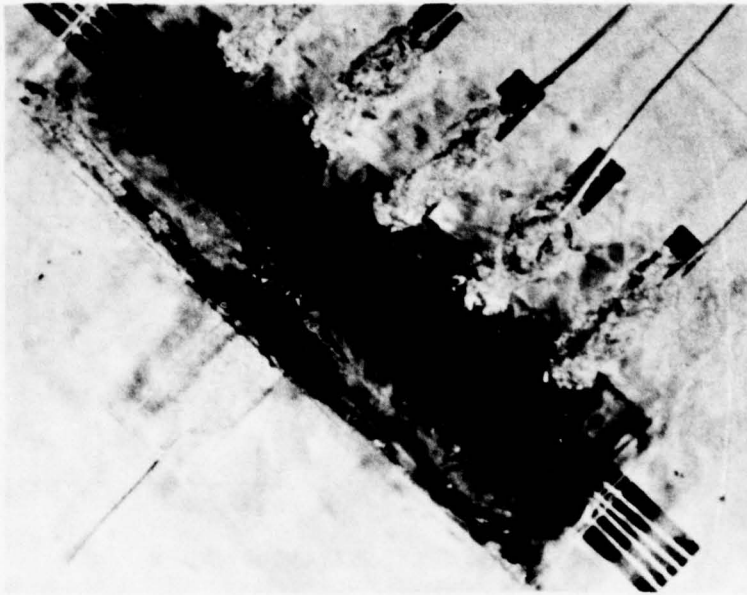
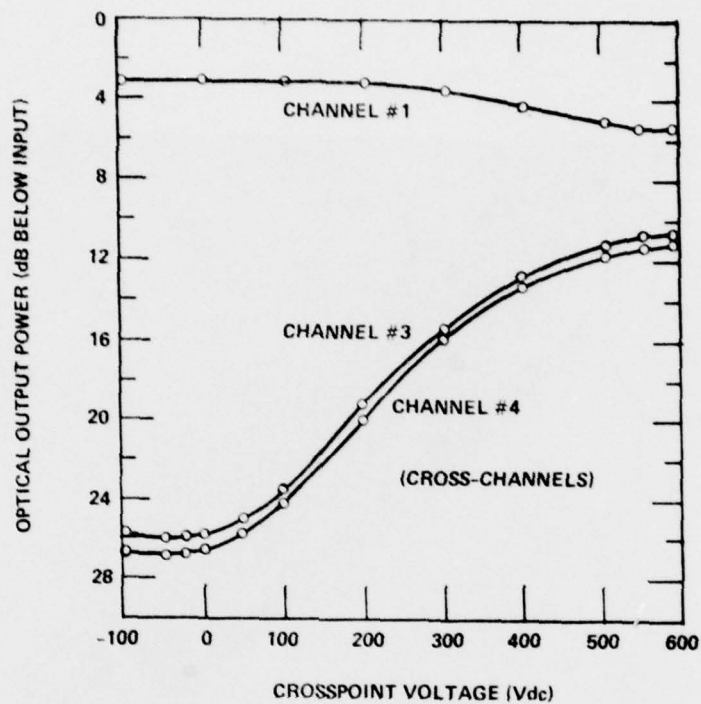


FIG. 28 Enlarged view of optical switching region of matrix.



78-28

FIG. 29 Measurements of switched optical power in 2 X 2 crossbar as a function of crosspoint addressing voltage.

the previous 9-mil channel width, 27-mil channel separation, 3.6° channel intersection angle, 1-mil deflector width, and 286-mil deflector length.

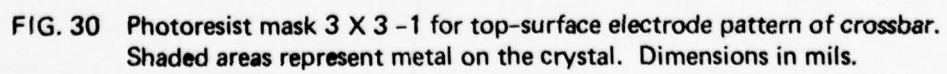
The top-surface mask 3x3-1 is shown in Fig. 30. A detailed view of each crosspoint is very similar to that shown in Fig. 23. The bottom-surface mask 3x3-2 for the common electrode is presented in Fig. 31. Again, the detail is like Fig. 24. The crosspoints are arrayed within a 5.0 cm x 0.2 cm region, although the crystal should be 6.6 cm x 1.0 cm to accommodate lengths of waveguide that come into and go out of the interaction region.

With the exception of the 3 x 3 matrix ends, which are angle-terminated, the remainder of the construction process very closely parallels that of the 2 x 2 array. Again, there is a window mask, 3x3-3 of Fig. 32, for preparing openings in the insulating resist layer, and a corresponding metal evaporation mask, 3x3-4 of Fig. 33, that delineates conductive paths going to the crosspoint bars. Section 7 and Appendix A tell more about how this matrix is made.

7. TECHNIQUES FOR DEVICE FABRICATION

Most of the constructional features can be seen by looking through the end-surface of the matrix (Fig. 34), although the drawing is somewhat schematic because there are several hidden lines and the crystal height has been exaggerated. The overall assembly process for the angle-terminated matrix is indicated symbolically in Fig. 35. Unlike our earlier crosspoints, a continuous glass top plate is not present and, in its stead, a thick (60 μ m) layer of insulating resist has been substituted. It has judiciously placed openings through which electrical contact is made to the switches.

During this contract, a number of modifications and improvements were made to the electro-optic device fabrication steps worked out on the preceding contract.¹ A definite process for matrix fabrication has evolved, and in Appendix A of this Report we give a detailed description of each processing step. During the last weeks of this contract, paraffin was substituted for glycolphthalate (see Appendix A), to permit a 40°C lowering of all processing temperatures.



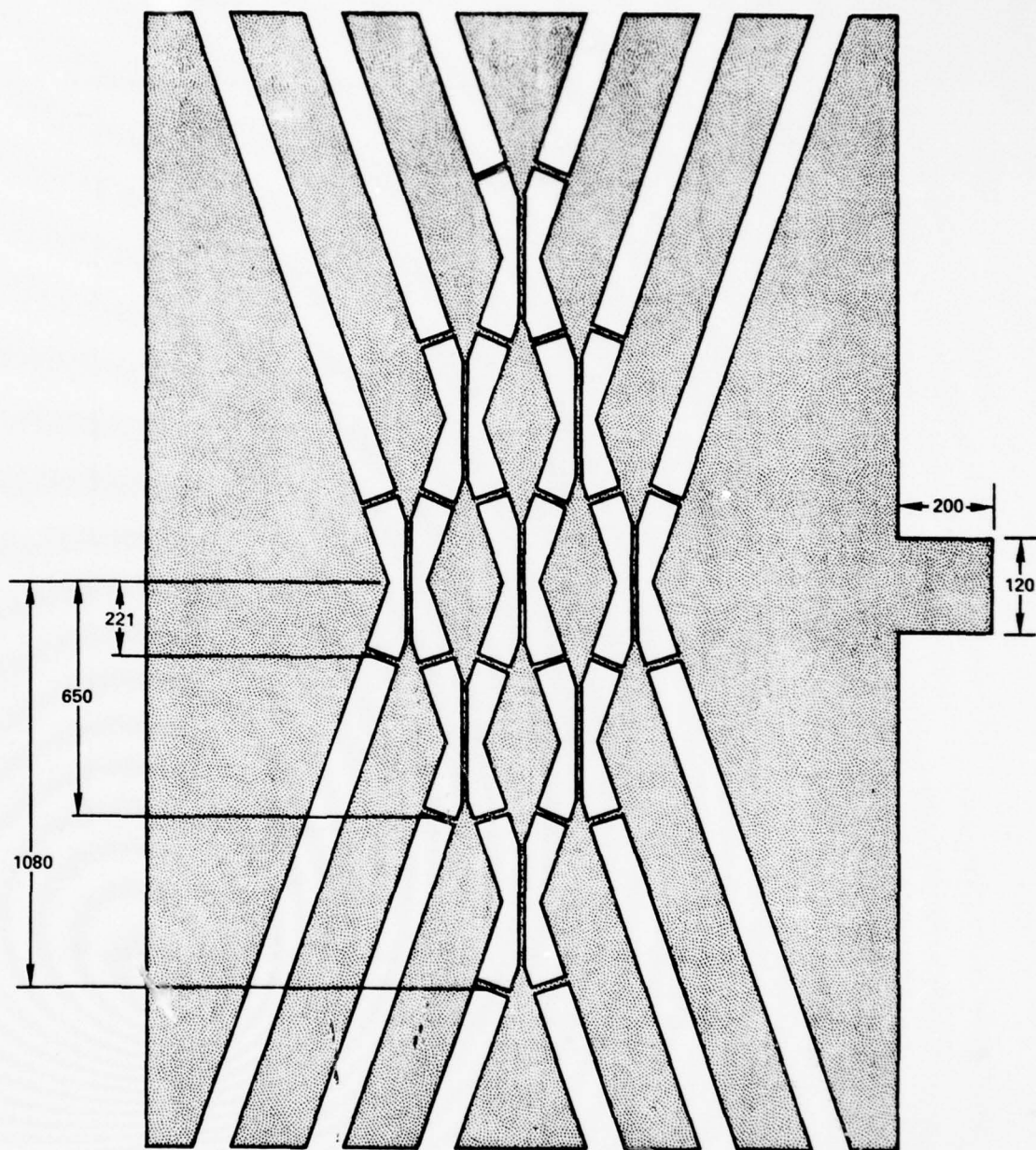


FIG. 31 Photoresist mask 3 X 3 -2 for bottom-surface electrode pattern of crossbar. Shaded areas represent metal on the crystal. Dimensions in mils.

78-30

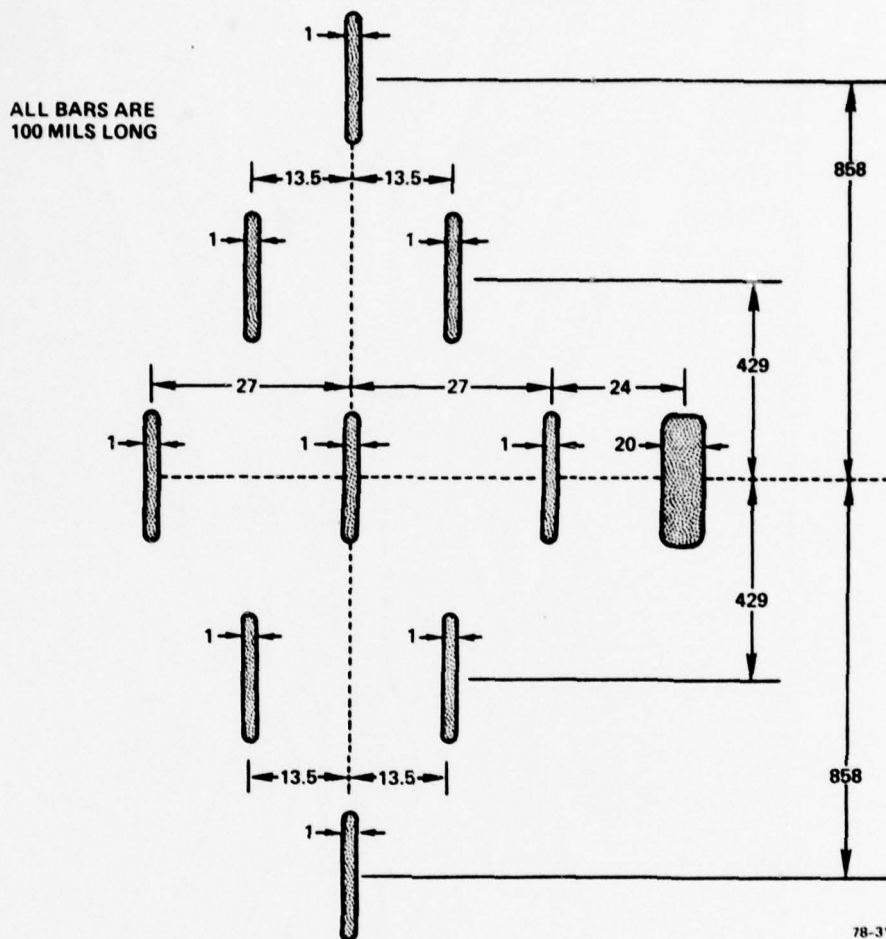


FIG. 32 Photoresist mask 3 X 3 -3 for making openings in insulating film covering 3 X 3 top-electrode pattern. Shaded areas represent windows registered on crosspoints. Dimensions in mils.

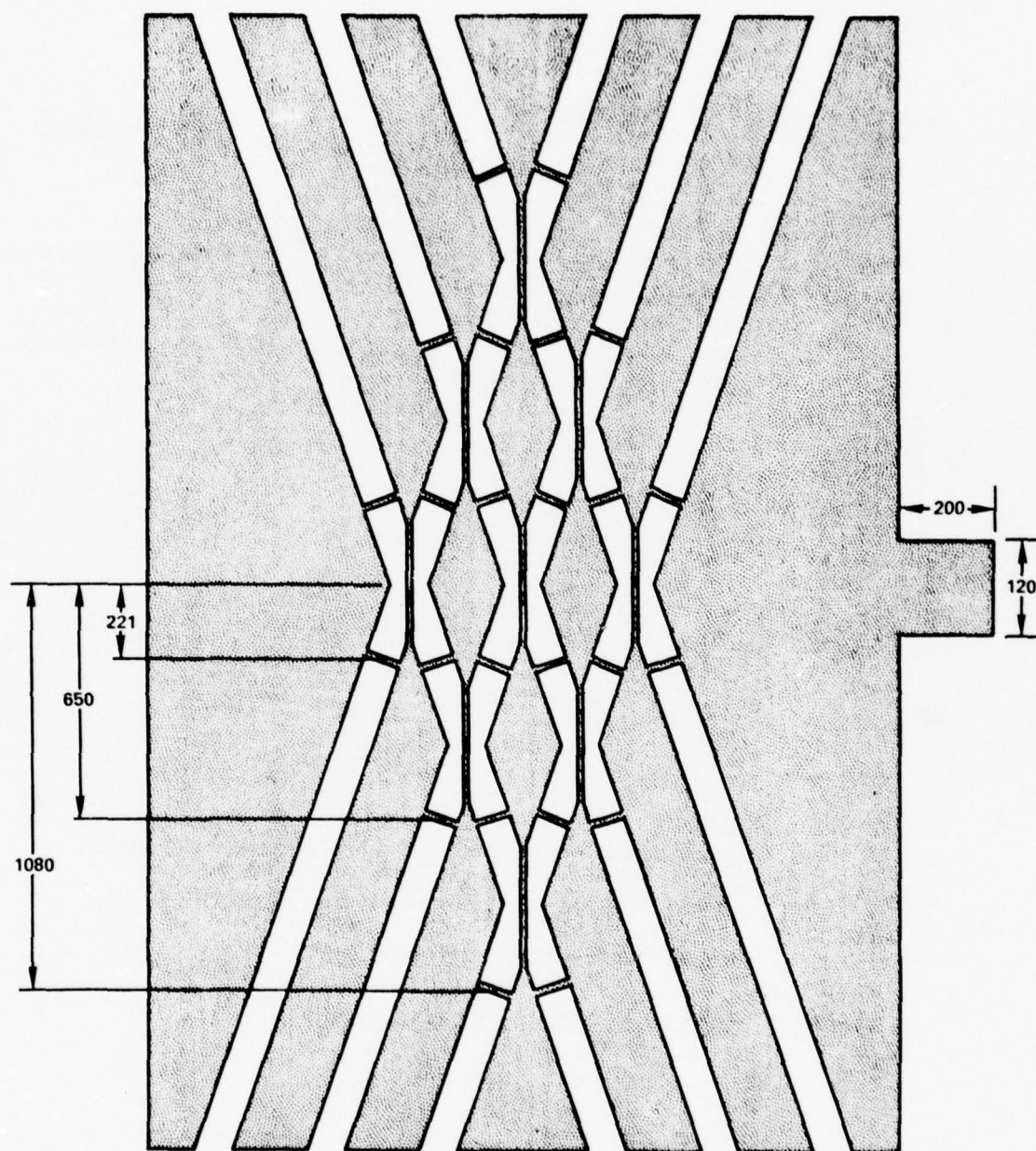


FIG. 31 Photoresist mask 3 X 3 -2 for bottom-surface electrode pattern of crossbar. Shaded areas represent metal on the crystal. Dimensions in mils.

78-30

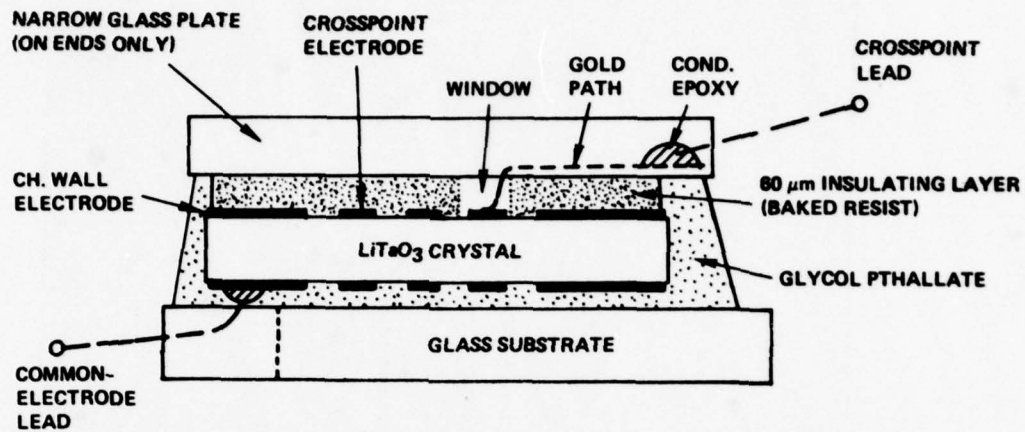


FIG. 34 End view of optical matrix.

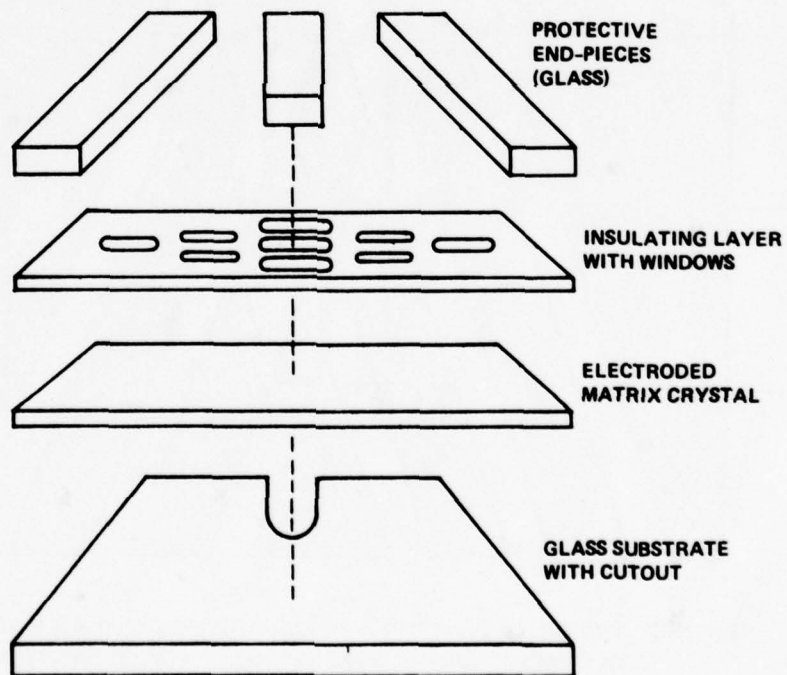


FIG. 35 Exploded view of angle-terminated matrix illustrating how the device is put together.

8. YIELD PROBLEM ON 3 x 3 MATRICES

The most serious problem encountered on this contract was the defect-free processing of large, fragile crystals. While 3-mil, 2.5-cm-long crystals are quite "manageable", the device yield decreases with increasing crystal length, dropping rapidly for lengths beyond 5.0 cm. Specifically, we found 90% yields for individual crosspoints on 2-cm plates and obtained 50% yields for 2 x 2 matrices of 4.0 to 5.0-cm dimension, but experienced yields of approximately 10% for larger samples. Ten large crystals, 6.6 cm x 1.0 cm x 0.0078 cm, were purchased for the 3 x 3 matrix and ten attempts were made to build it. This Section documents what happened in each case. Looking at the results as a whole, the attempts were only partly successful because the best matrices had seven out of nine crosspoints operative. Device processing was hampered by accidents and by the low cumulative probability of successfully carrying out a long sequence of processing steps.

The 3 x 3 device history is as follows. Early samples were mounted on a sturdy glass substrate of unknown composition, possibly pyrex or fused quartz. The difference between the x-y thermal expansion coefficients of LiTaO_3 (16 ppm/deg C) and the substrate (~5ppm/deg C) created stresses that led to cracking of the initial samples during the heat-cycle needed to loosen the crystal bonding cement (See Appendix A). This difficulty was partially alleviated by changing the substrate material to soda-lime glass, ordinary microscope slides, whose expansion coefficient was approximately half that of LiTaO_3 . Glasses with yet higher thermal expansion coefficients (~3/4 that of LiTaO_3) are available commercially but they could not be procured in time to be used on this contract. Paraffin, a softer bonding agent, also helped because of its lower processing temperatures. We were able, after a learning process on small crystals, to avoid cracking 3 x 3's when sliding the crystal from one glass substrate to another. However, cracking did occur during metal liftoff when rapid evaporation of acetone led to a fast cooldown of the crystal. We solved this problem by transferring the sample quickly from the acetone bath to a total-immersion water bath. One sample cracked accidentally when incompletely dried resist stuck to the photomask. Two other samples succumbed to accidental dropping.

Samples 8 and 9 each developed a crack near one end of the crystal, but since 5.0 cm of crystal remained, the samples were suitable for subsequent 3 x 2 matrix array fabrication. After stripping off the original metalizations, we

"recycled" both samples and went through the processing without difficulty except for the insulating-film problem discussed below.

Sample 10 remained intact over its entire length. This is seen in the Fig. 36 photograph, taken after the second photolithography step (part E of appendix A). Then we completed the angle-cutting, the optical polishing and all the remaining steps on Sample 10 which finally had the appearance shown in Fig 37. Unfortunately, Sample 10 was later accidentally damaged with a solvent that rendered four crosspoints short-circuited to the waveguide electrodes.

If we examine the fabrication critically and look for weak links in the processing chain, we would pinpoint the insulating-film step. The 3×3 crystal is not well-enough encapsulated because the insulating layer is vulnerable to a number of environmental hazards. It is susceptible to organic solvents, despite the fact that it is thoroughly baked to drive out moisture. A stray drop of acetone can wipe out an insulating crossover if it lands on the wrong place on the film. Also, we found that the film is attacked by small amounts of trichloroethylene that leach out of conductive epoxy. A crosspoint in sample 9 was damaged (shorted) when we patched a gold path with small dab of conductive epoxy.

A. Experimental Crystals

Extensive experiments have been carried out on Samples 8 and 9 which have the largest number of functional crosspoints. Both devices are angle-terminated. After attaching fiber trios to both ends of Sample 8, we observed slow fluctuations in the fiber output, attributable to liquid flow (or possibly to heating effects) at the second crystal-to-fiber coupling surface. There were periods when the optical throughputs stabilized and the switching performance was good. We gathered data at those times. We also began to make measurements on Sample 9 before cementing the fibers in place, but we accidentally squeezed the crystal between two micropositioners with considerable pressure, inducing two hairline cracks in the crystal that increased the background light considerably and shorted out an additional crosspoint. The results obtained on all ten 3×3 matrix samples are summarized in Table 2.

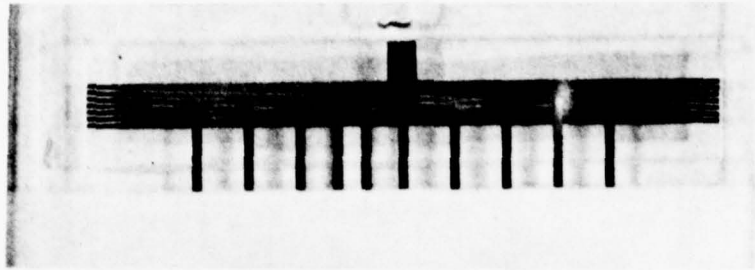


FIG. 36 Matrix crystal (3 X 3 sample 10) in which the desired processing via masks 1—4 has been carried out on both sides.

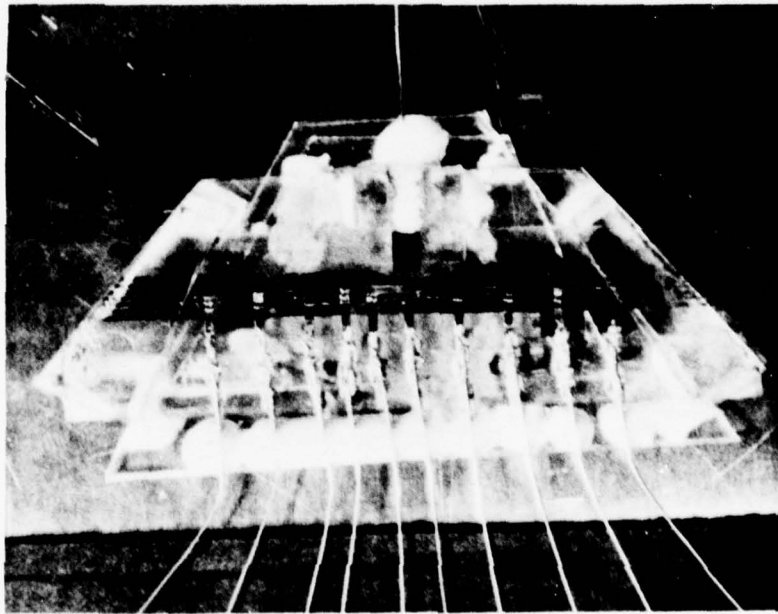


FIG. 37 Experimental model of completely processed multimode optical matrix (3 X 3 sample 10). Matrix ends have been cut at 39.4° to the channel axes and electrical leads have been attached.

Crystal Designation	Final Length (cm)	Percent Completion of Device Processing Steps	Comments
1	3.6	15	Crystal cracked during heating cycle
2	4.0	20	ditto
3	4.5	20	Crystal cracked when it accidentally stuck to photomask
4,6	3.8	40	Crystal cracked during acetone-controlled liftoff
5	---	80	Sample accidentally dropped and broken
7	4.5	85	Sample cracked by accidental pressure on top surface
8	5.1	100	3 x 2 matrix successfully made. Fluctuations in second matrix/fiber interface. Seven crosspoints operative.
9	5.2	100	3 x 2 matrix successfully made. Sample cracked later by accidental lateral pressure. Six crosspoints operative.
10	6.4	100	3 x 3 matrix successfully made, but four crosspoints later shorted by solvent spillage. Five crosspoints operative.

Table 2. Status of ten 3 x 3 matrix devices prepared in LiTaO_3 crystals.

9. FIBER ARRAY TERMINATIONS

The all-silica Corning fibers were chosen because of their low loss and relatively low NA, which is advantageous for switching. These step-index fibers have a 125- μ m cladding diameter and 85- μ m-diam cores.

Fiber trios are set in parallel microgrooves cut in a flat glass substrate to form planar linear fiber arrays. Although V-grooves provided by preferential etching of silicon will hold fibers with precise spacing, we obtained a good spacing accuracy by cutting shallow rectangular slots, 5.0 mils wide and 3.2 mils deep, using a programmable saw made by the Tempress Company. The desired groove width was obtained by experimentation with several microsaw blades. The saw blade can step horizontally in 0.5 mil increments and vertically in 0.1 mil steps.

The 2.6-fold collimation factor and the 27-mil matrix channel spacing imply a fiber spacing of 10.4 mils. Since the saw will only provide a 10.5 mil spacing, we instead employed a collimation factor of 2.57, and put the fibers 10.5 mils apart, center-to-center.

Turning to the graph of Fig 10, we find that the matrix should be cut at 39.4° to its channel axes, and that the fiber arrays should be cut and polished at 72.6° to the fiber axes, for $f = 2.57$.

After pressing the monofibers into their grooves, we covered them with a thin coating of Epo-Teck #330 epoxy. We then pressed a second glass plate on the coated fibers and cured the epoxy. This glass "sandwich" was then cut at the desired 72.6° angle, (Fig 38) with a diamond-blade saw giving two arrays. Prior to cutting, the fibers were protected with a plastic jacket that was glued into beveled end-regions on the 3 x 1" plates, as shown in Fig 38. A series of polishing-wheel steps, done manually using a brass fixture and alumina solutions, provided the desired optical finish. Photomicrographs of the polished angle-terminated input and output fiber arrays are presented in Fig 39, and a macroscopic view of the completed fiber terminations is presented in Fig 40.

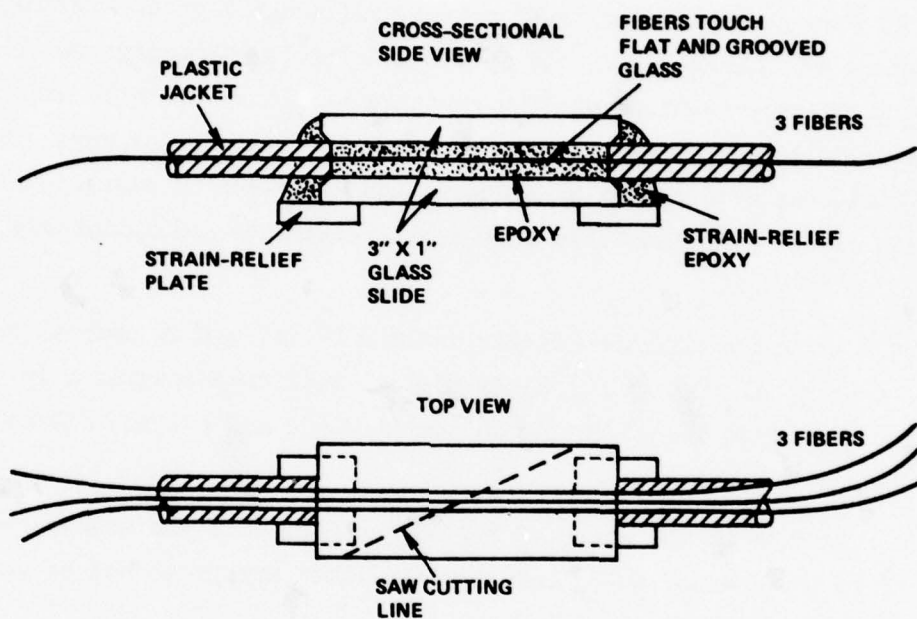


FIG. 38 Two views of 3-fiber arrays showing how the angle-termination is done simultaneously on two arrays.

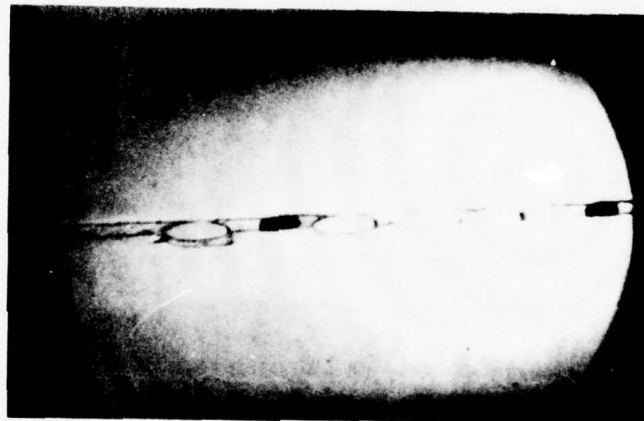
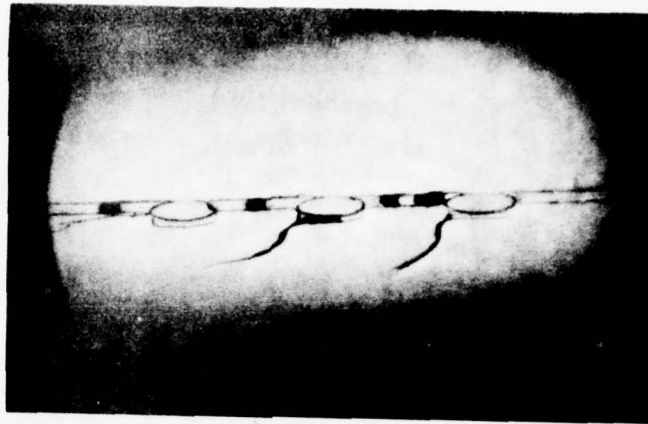


FIG. 39 Magnified end-views of actual 3-fiber arrays, input and output trios, terminated at 72° to the fiber axes.

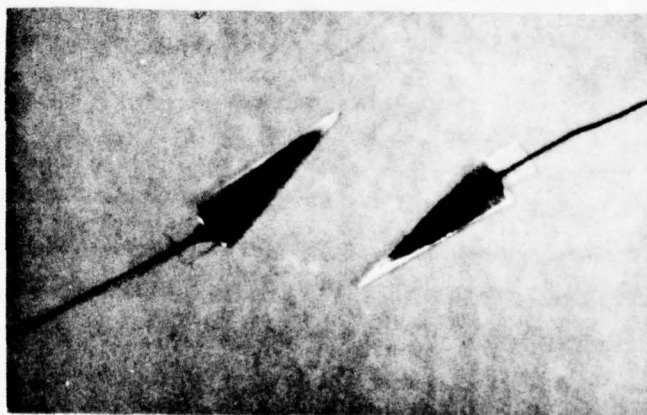


FIG. 40 Top view of terminated fiber arrays, ready for matrix coupling.

10. CONTROL ELECTRONICS

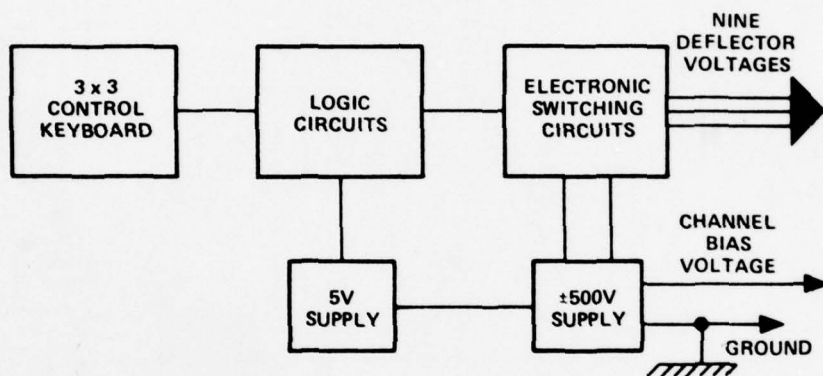
A 3 x 3 matrix control box has been built so that the optical linkages in the fiber-optic intercom can be selected manually. The box provides binary-state voltages (V_a or V_b) to each of nine optical crosspoints, as well as the waveguide bias voltage. Solid-state components are used throughout and the box is self-contained since it includes two miniature power supplies plus the addressing keyboard.

Fig. 41 shows a block diagram of the control box. Optical connections are controlled by pushbuttons and low-voltage logic circuits are provided to "lock out" party-line calls in which one fiber input is coupled to several fiber outputs, or vice versa. Switching voltages in the 0- 500 Vdc range are supplied, plus a 0- 500 Vdc bias. Connection is made to the common electrode of the matrix.

Three potentiometers are located at the rear panel of the box for the adjustment of V_a from 0 to +500 Vdc and V_b from -500 to 0 V dc (these voltages usually have opposite polarity) and for the adjustment of V_w from -500 to +500 Vdc. A polarity switch is provided to reverse the signs of V_a and V_b .

Analogous to crosspoints, the control keys are arranged in a row-column array. A red, yellow, or green LED lights up (one color per row) when a particular crosspoint has been turned on, and only one crosspoint per row (and one per column) can be selected (at most 3 out of 9), giving the six different input-output pairings. A "matrix clear" switch has also been provided. Initially, it applies a voltage V_a to all nine crosspoints, and later, after a pattern of conversations has been set up, the clearing switch can erase the pattern and allow a new one to be established.

The box's circuit diagram is fairly complicated due to the IC logic elements that exclude party-line calls and to the nine-fold replication. We have divided the circuit diagram into two parts. The first section, presented in Fig. 42, shows the transistorized keyboard pushbuttons, matrix clear switch, polarity switch, logic and TTL gates whose outputs are converted to higher voltage levels. The 5V supply is not shown. The second section, presented in Fig. 43, shows the discrete pnp and npn transistors that actuate the crosspoints, plus the associated dc supply for V_a and V_b .



78-35

FIG. 41 Block diagram of optical matrix control box including self-contained power supplies.

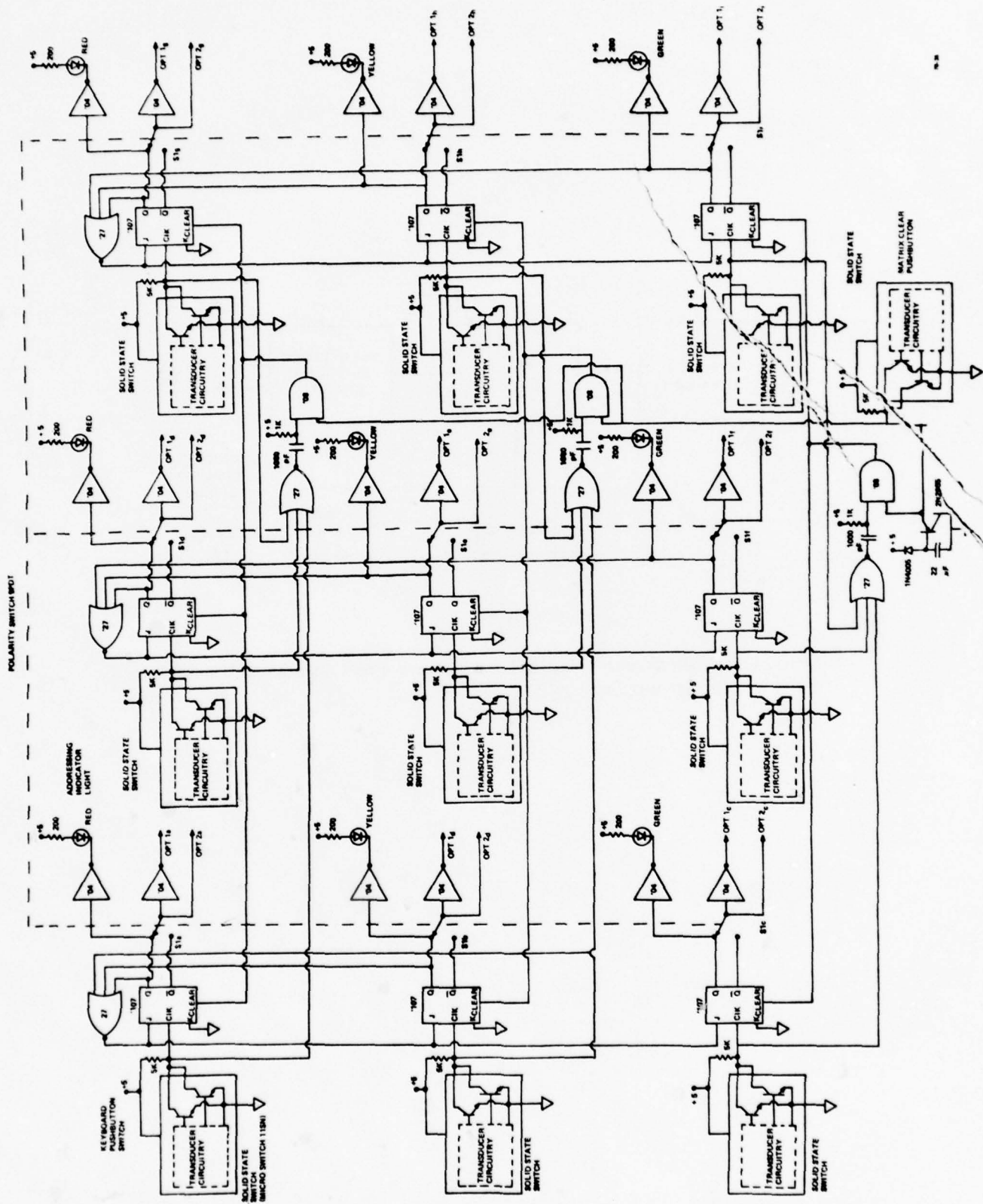


FIG. 42 Circuit diagram of 3 X 3 optical matrix control box showing all five-volt switching circuits.

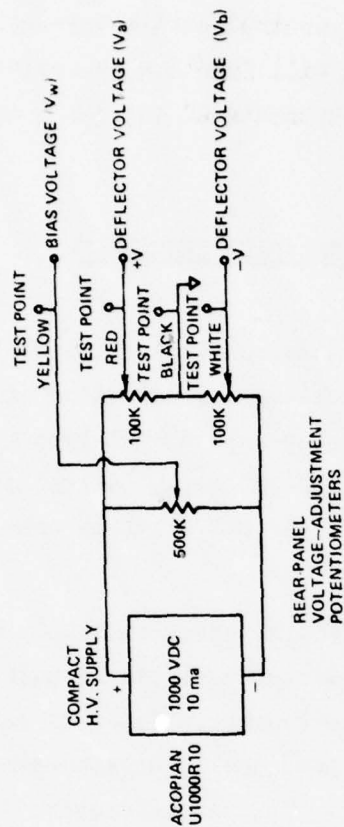
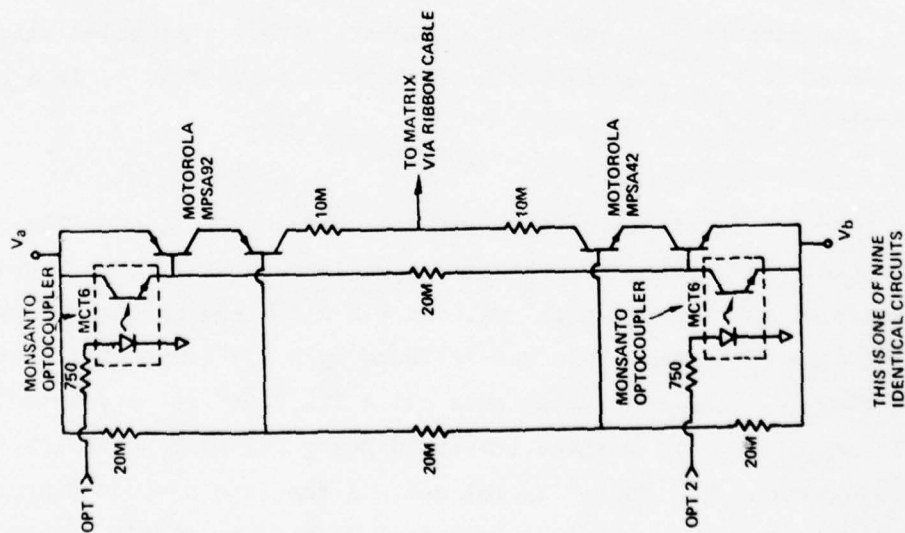


FIG. 43 Remainder of control box: transistor switching circuits and associated power supply for controlling optical crosspoints. These circuits are actuated by the TTL gates in Fig. 42.

Photographs of the completed control unit are presented in Fig. 44. It is interesting to note that the box will function as desired for each of the various 2 x 2 matrices that are sub-components of the 3 x 3 array.

11. OPTICAL DATA TERMINALS

A. Transmitters

Three independent infrared sources, plus drive circuits, were mounted in one chassis box to facilitate a bench-top demonstration of the system. The emitters chosen were Plessey HR 952 etched-well Burrus-type LEDs having maximum emission at the 0.90 μm wavelength. A 30-cm length (pigtail) of 85- μm core, 0.15NA low-loss monofiber was bonded to the LED emitting area with crystal-clear epoxy.

Rather than using external data sources, we simply made internal circuit arrangements so that each LED put out a steady stream of pulses, with optical bit rates in the ratios 1:2:4 for the three sources. The data rates were determined by the receiver bandwidths. Fig. 45 shows the integrated-circuit logic and IC drivers for the transmitting terminals. The potentiometers were set so that each LED injected 32 μW of power into its fiber.

Fig. 46 shows an internal view of the transmitter assembly including the copper heat sink for each LED and the glass alignment sleeve that aided attachment of the pigtail. The chassis contains a miniature 5V supply. Fig. 47 is a photograph of the completed unit.

B. Receivers

Three infrared receivers were put in one chassis box to keep the system condensed for demonstration purposes. We used a Bell-and-Howell/Devar type-529 hybridized detector consisting of a 5 mm^2 silicon PIN diode and an operational amplifier mounted in a TO-5 can. This was followed by a 733 video amplifier IC and a 311 Comparator IC. The comparator puts out a TTL "one" for any detected signal above the threshold, the voltage threshold being set by a potentiometer. For signals below threshold, a "zero" is put out. A complete circuit diagram of the optical receiver, including the self-contained 15 V power supply, is presented in Fig. 48.

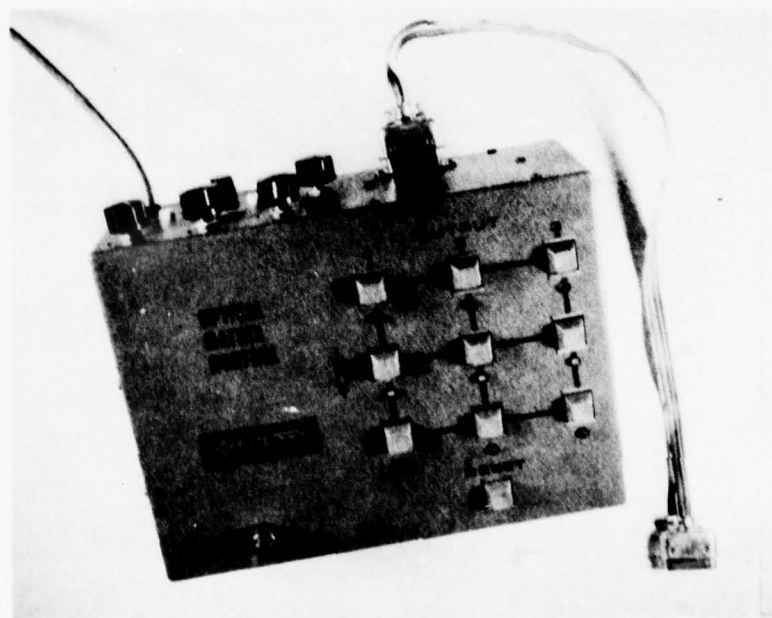
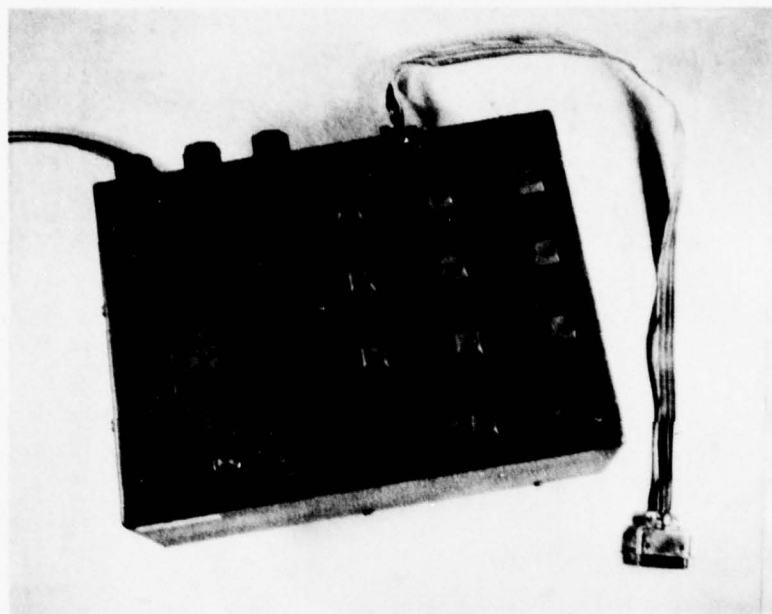


FIG. 44 Two views of 3 X 3 matrix control box showing keyboard, backpanel adjustments, and 11-wire connector.

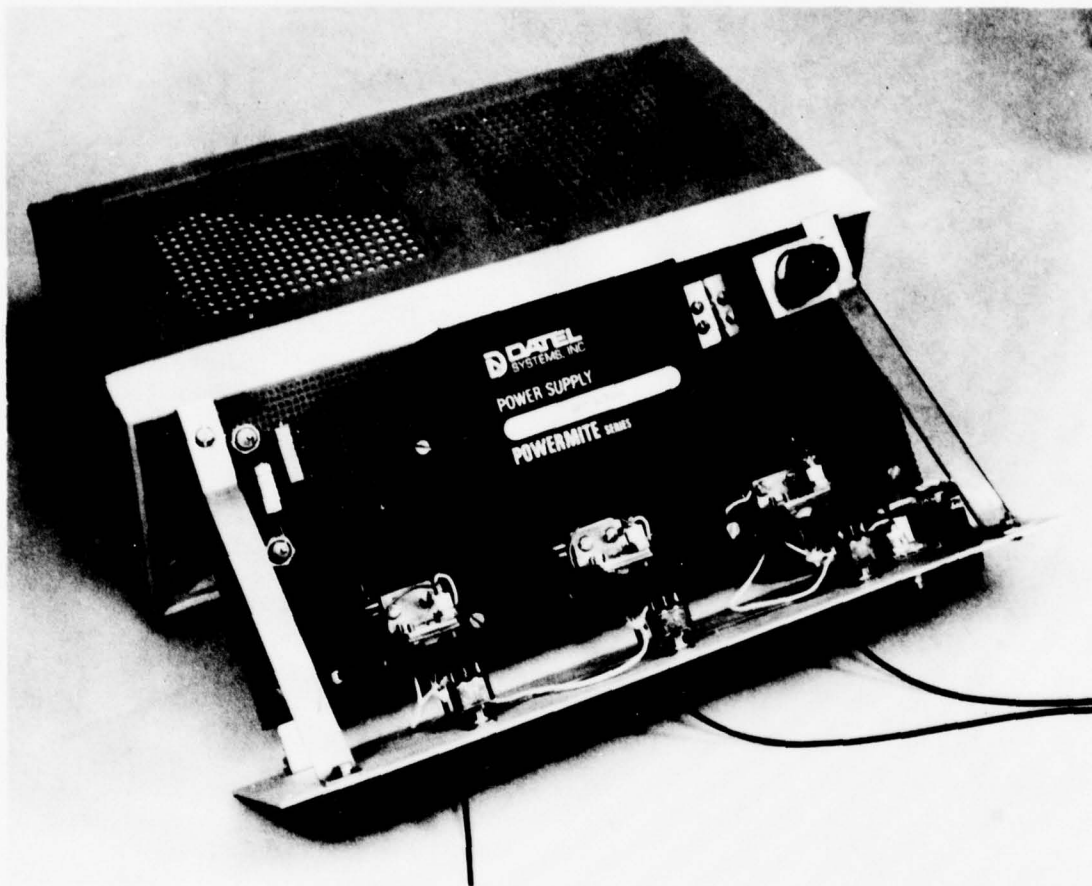


FIG. 46 Inside view of experimental 3-terminal box containing independent GaAs LED data sources.

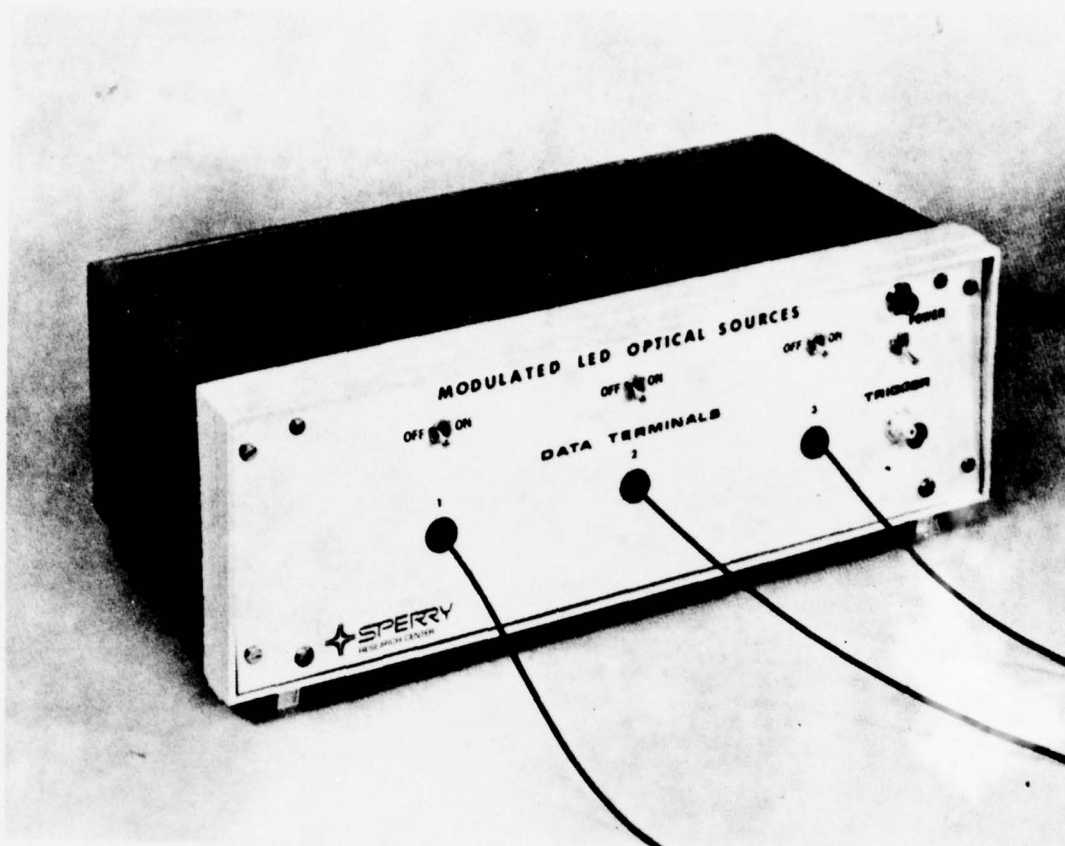


FIG. 47 Multiple sources for optical intercom system.

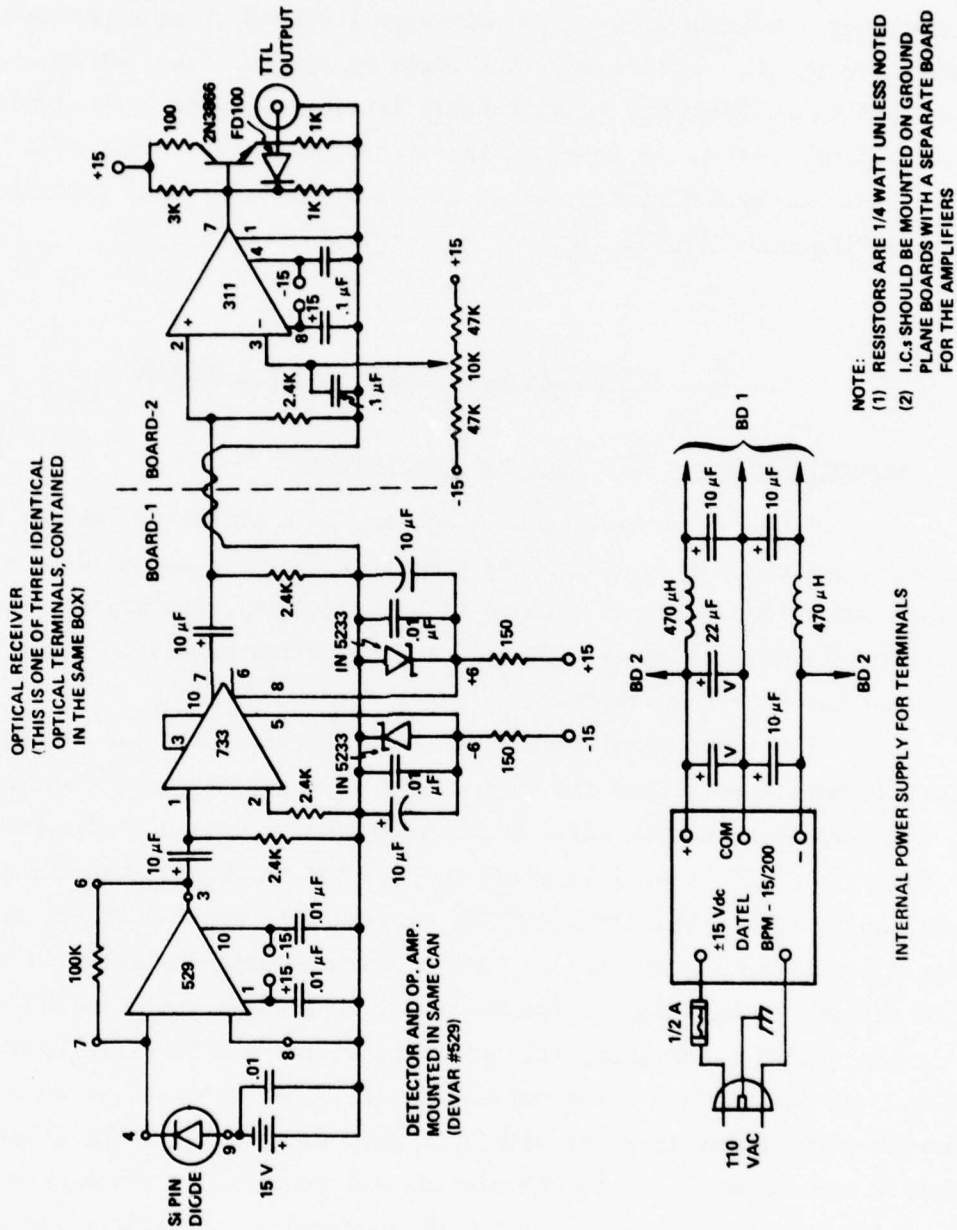


FIG. 48 Circuit diagram of optical receivers for intercom system.

The Fig. 49 photograph shows an inside view of the optical receiver box including both circuit boards. An aluminum alignment sleeve containing a set-screw is placed directly in front of each photodetector, coaxial with it. In this way, the incoming optical fiber strand, which is centered in a 1/8"-diam. brass-ferrule termination, can be brought in to the central area of the detector and locked in place. Stray room light is also kept out by the arrangement. A view of the completed multi-receiver unit is presented in Fig. 50.

12. EXPERIMENTAL RESULTS ON 3 x 3 SYSTEM

A. Assembly of Fiber-Matrix-Fiber Combination

Using a triangular glass spacer, we elevated the matrix 0.1" from an aluminum mounting plate. This permitted the free up-and-down movement of fiber arrays brought into contact with the matrix. Mechanical x-y-z- ϕ adjustments could then be made to bring the fiber axes into proper relationship to the matrix channels.

The input termination containing three fibers was attached with double-sided tape to the arm of an x-y-z micropositioner and was moved into contact with the matrix end. We then injected a drop of index-matching anti-reflection fluid ($n = 1.62$ in the red) at the interface, the liquid being held there by capillary action. By exciting the various fibers with a He-Ne laser and centering the fibers in the electro-optic channels, we maximized the channel throughputs collectively. This process was repeated by bringing the second fiber array into position at the matrix exits (where the AR fluid was included). After optimizing all fiber outputs, we bonded both arrays permanently in place with Torr Seal epoxy. Next, the fiber-coupled matrix was inserted in its chassis box and cemented in place, with leads from the multi-wire chassis connector soldered to the matrix wires. Figure 51 is a photograph of the completed fiber-coupled matrix in its aluminum container.

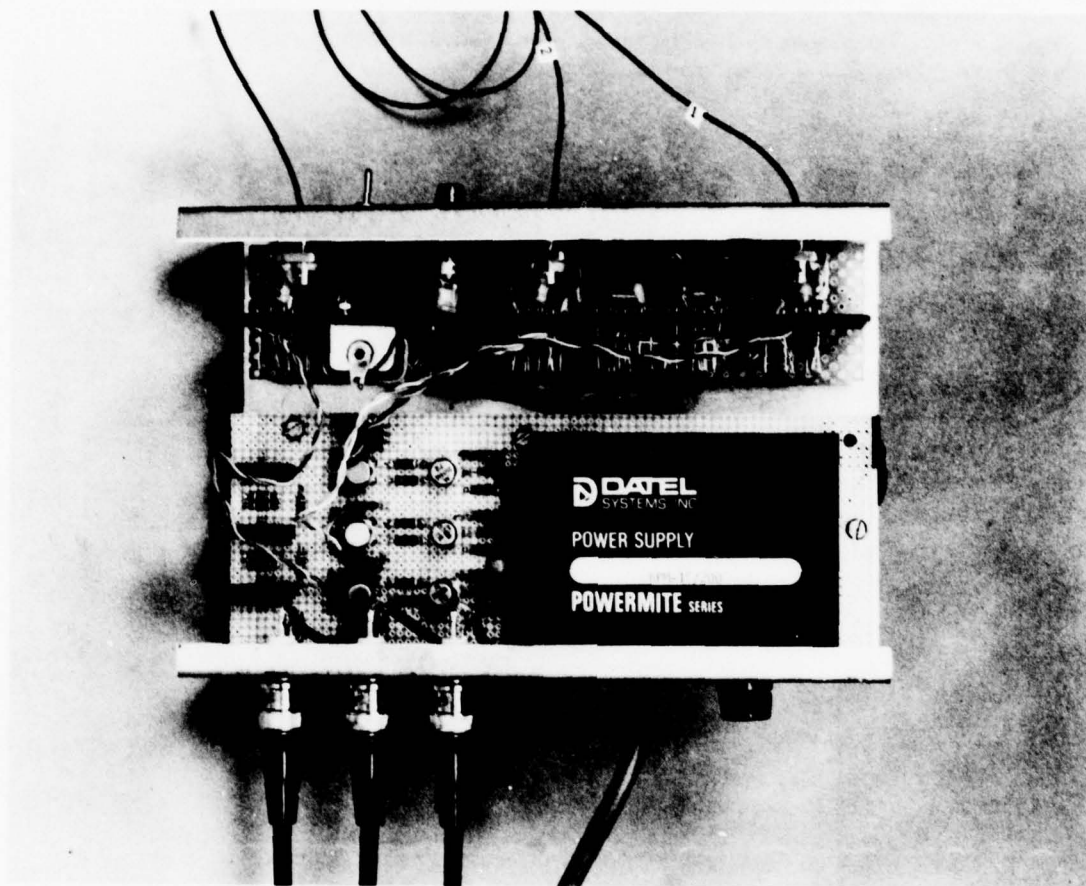


FIG. 49 Inside view of experimental 3-terminal box containing independent infrared detector/preamps and digital signal-processing circuits.

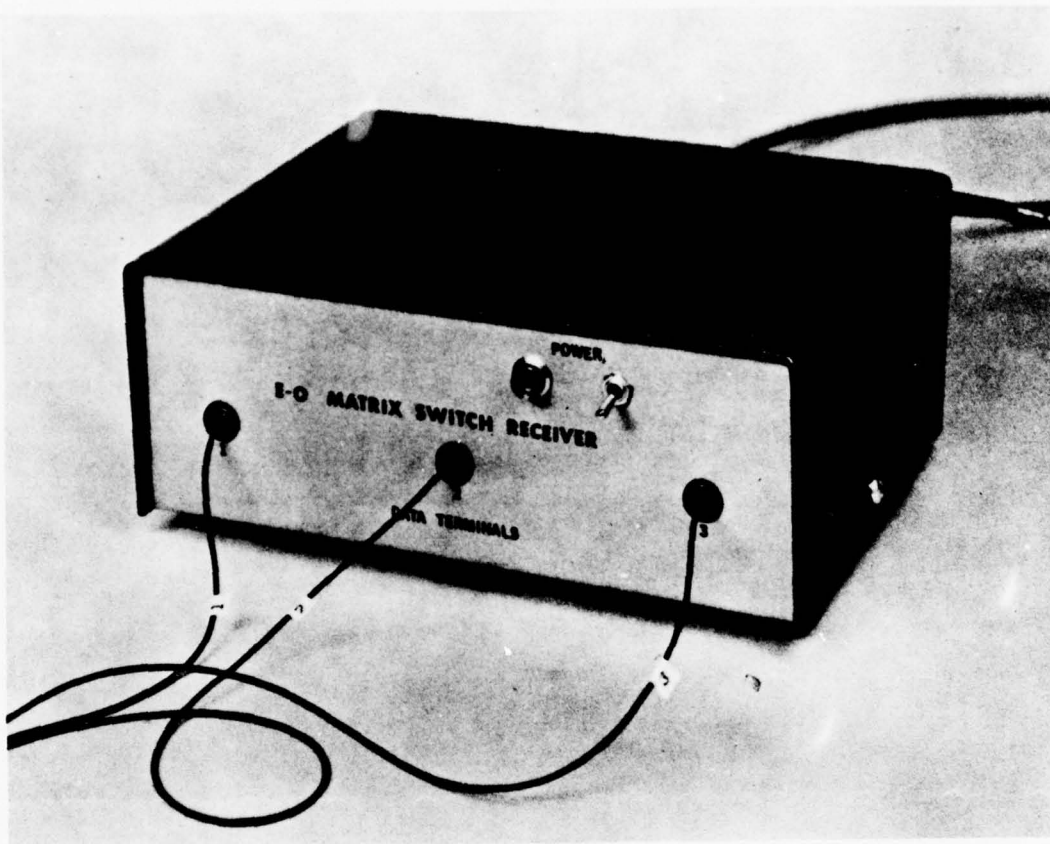


FIG. 50 Multiple receivers for optical intercom system.

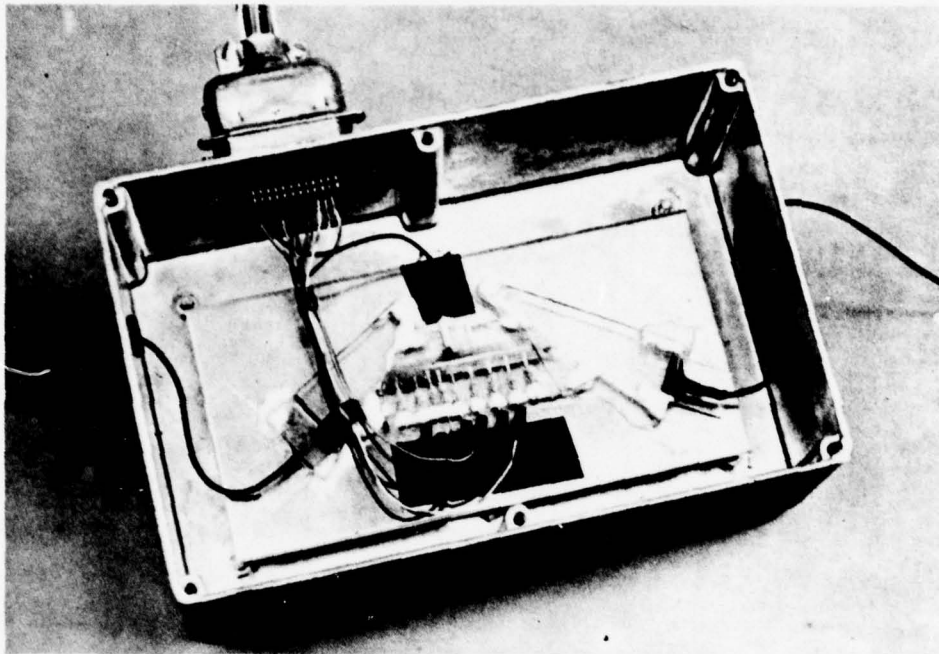


FIG. 51 Experimental model of multimode 3 X 2 fiber-optical-matrix switch including electrical control wires.

B. Performance Measurements

To get a visual indication of how the fiber/matrix/fiber combination was performing, we excited one of the input fibers (filling its 0.15 NA with 0.63 μm light) and examined the three fiber outputs, imaged on a white viewing screen, during various electro-optic addressing situations. The results are presented in the composite photograph of Fig. 52, which includes five exposures. In the Fig. 52 experiment, the unselected crosspoints had a voltage V_a applied to them. For the channel-3 input, all three crosspoints in the third row were addressed with voltage V_b (top photo); then one crosspoint at a time in that row was turned on with V_b (middle three photos); then the output with all crosspoints having V_a applied was observed (bottom photo). The desired three-fold switching is clearly seen. Some optical crosstalk is also present (quantitative results below).

We next measured optical insertion loss. The matrix-switched fiber output power was determined with a silicon pin detector and compared to the matrix fiber input power. When examining the input, we attenuated the optical input level with a calibrated 18 dB filter and placed the photodetector at the focal spot (minimum waist) of the laser beam directed into the fiber. The optical insertion loss of the fully addressed fiber/matrix/fiber from all contributions was 21 dB, but the actual loss was 1 to 2 dB lower than this because the fiber did not capture all of the convergent input light. Because the absolute responsibility of the infrared receiver was not known, the infrared loss was not determined; however, since LiTaO_3 is highly transparent in the near-infrared, we believe the matrix insertion loss at 0.90 μm is equal to, or less than, that at 0.63 μm .

From previous experiments, the breakdown strength of the 75 μm crystal plate is 550 to 600 V dc. To give a margin of safety, we kept the waveguide bias voltage V_w well below this level. Similarly, the 60 μm insulating film can stand off about 450 V dc, and we held the film voltage below this critical level, at 340 V dc, to avoid dielectric breakdown. The voltage across the film is $V_w - V_a$, and we chose individual values of $V_w = +320$ V dc and $V_a = -20$ V dc. (The small negative voltage is useful in suppressing background light.)

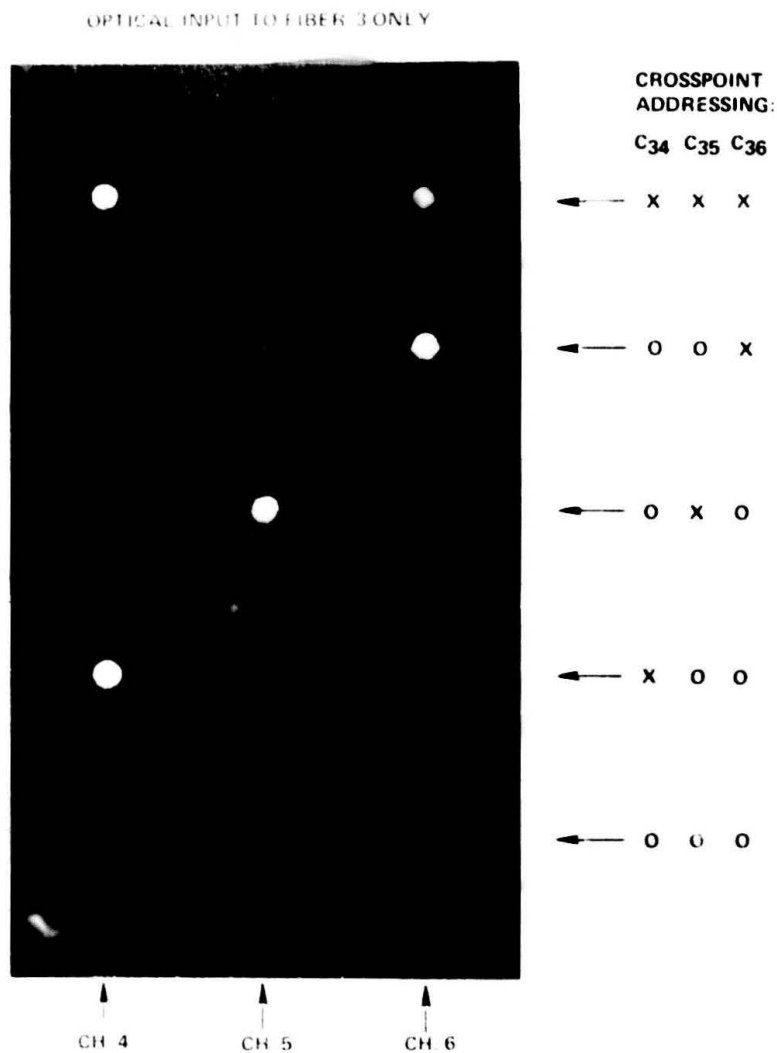


FIG. 52 Switched optical outputs from three fibers coupled to 3 X 2 matrix sample 8. One of the input fibers coupled to the matrix is excited with unpolarized red light. In the addressing, the symbol "X" denotes the voltage V_B applied, while "O" represents V_A applied.

The matrix currents are quite small and are primarily capacitive charging currents. A set of capacitance measurements at 1 kHz revealed that the capacitance of each optical crosspoint is 19 pF, and that the inter-electrode capacitance between crosspoints is 9 pF. When driven by a 50 Ω controller, the RC time of the switching electrodes is 1 ns. The figure of merit, $\frac{1}{2}CV^2$, is approximately 2 W/MHz.

We next inserted the brass-ferrule fiber terminations into the three receiving terminals and did a scribe-and-break operation on the free ends of the matrix input fibers, prior to inserting them into connectors attached to the transmitting-terminal pigtails. In this way, we assembled the fiber-optic communication system. A photograph of the complete 6-terminal matrix-switched optical intercom is shown in Fig. 53.

In the GaAs LED drive circuits, trimmers were set so that the infrared power emerging from each of the three fiber pigtails was 32 μ W. This 32 μ W excitation gave adequate signal-to-noise ratios at the receivers.

The hybrid diode/op-amp detectors are capable of demodulating digital optical data at 20 megabits/s (Mbps), and the fiber/matrix/fiber combination can easily pass 100 Mbps data. However, because of the ~ 0.3 μ W signal levels at the receivers, the detectors need to be set for maximum sensitivity. This, in turn, requires a detector load resistance of 100 k Ω which reduces the detector bandwidth to 0.5 MHz. To provide optical signaling compatible with this bandwidth, we set up 0.4 Mbps square-wave modulation on the channel-1 input radiation and set the channel-2 and 3 data rates at 0.2 and 0.1 Mbps, respectively, to distinguish them from each other. Figure 54 presents the optical signal waveforms (current waveforms in the LEDs). Because the detector response is rolling off at these bit rates, the observed output signals appear sinusoidal at the receiver, rather than square.

Optical crosstalk levels in the multimode communication system varied slightly from channel to channel and depended slightly upon which matrix configuration was chosen. The observed crosstalk level ($\lambda = 0.90$ μ m) ranged from -10 dB to -5 dB. Averaged over all matrix outputs, the optical extinction ratio was -8 dB when one LED source transmitted information.

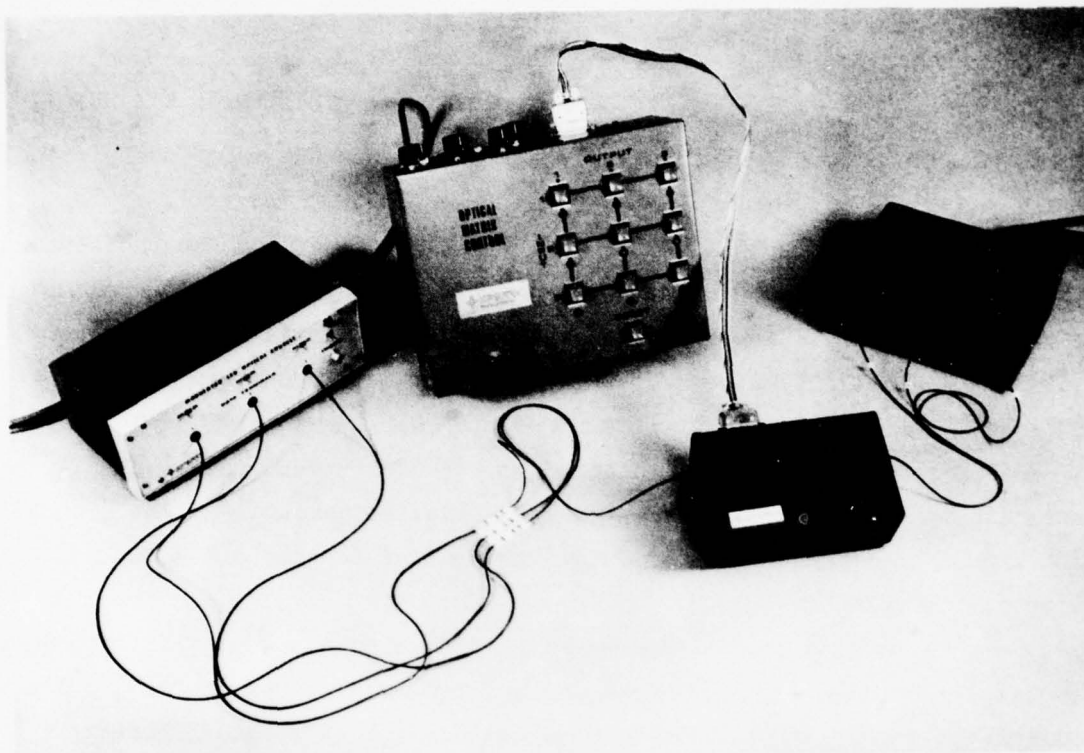


FIG. 53 Experimental multimode six-terminal crossbar-switched fiber-optic intercom system delivered to RADC/ETSL.

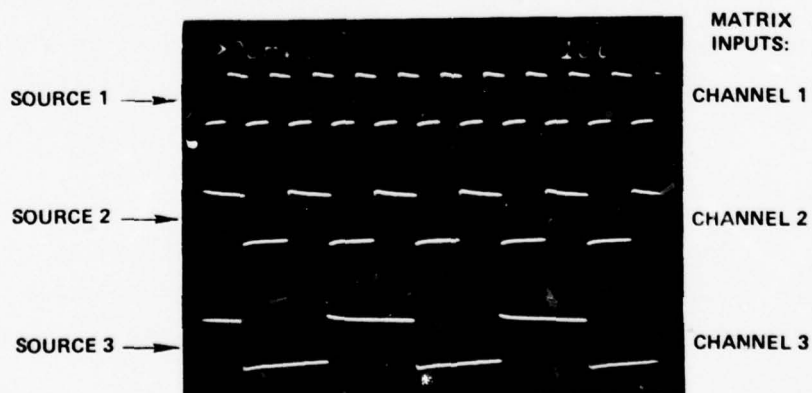


FIG. 54 Modulated $0.90\ \mu\text{m}$ light from each of the GaAs LED sources.

With the control keyboard, the matrix responded very quickly. Of course, the inherent matrix switching speeds are many orders-of-magnitude faster than can be seen by eye. Table 3 summarizes the experimental results described thus far.

To conclude this chapter, we shall show oscilloscope photographs of typical results for the intercom system using matrix 8. As mentioned earlier, the optical intensities emanating from channels 4, 5, and 6 of sample 8 moved slowly up and down with respect to one another due to an intermittent fiber/matrix interface. Photographs were taken during high-transmission conditions. In showing the receiver waveforms, we display the analog output of the 733 video amplifier (Fig. 48) as well as the digital TTL signal from the comparator (with the voltage threshold set at an appropriate value).

With data sources 1 and 3 turned on simultaneously, Fig. 55 shows the experimental 2 x 2 matrix switching found as a subset of the 3 x 2 capabilities. The figure indicates which combination of keyboard buttons (3 out of 9) was pushed in each case. In Fig. 55, the analog signal levels triggered three out of four comparator signals. The results of Figs. 56 and 57 are found by turning on data source 2 alone, or 3 alone, respectively. As one changes the set of addressed crosspoints, one can see the optical signal "shift" from channel 4 to channel 6 (Fig. 57), or from channel 5 to 6 (Fig. 56). The signal-to-crosstalk ratio is moderately high in Fig. 57.

13. DISCUSSION

The transition from individual electro-optic switches to 2 x 2 arrays went smoothly. Problems first cropped up in the larger 6.6-cm crystals for the 3 x 3 array because of their fragility and because of the larger number of processing steps.

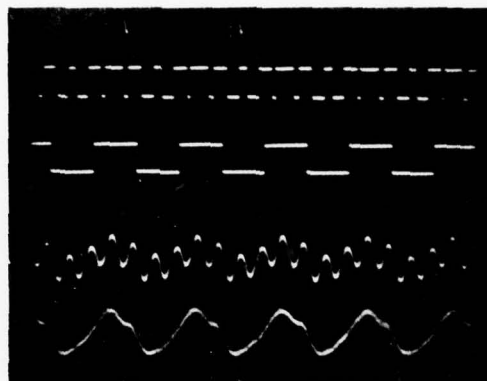
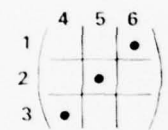
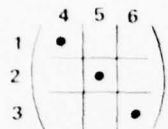
Apart from difficulties experienced with the 3 x 3 crystal, the other portions of the matrix-switched multiterminal fiber-optic communication system worked quite well, including the "hardware" (electrical control circuitry, keyboard, etc.) and the "functions" (the switching of incoherent, unpolarized infrared light).

Table 3. Measured performance of angle-coupled fiber/matrix/fiber switch.

Parameter	Result
Optical insertion loss of fully addressed 3 x 2 matrix	19 dB
Optical crosstalk at matrix outputs	-8 dB
Maximum permissible addressing voltages	$V_w = 550 \text{ Vdc}$, $V_b = 550 \text{ Vdc}$, $V_a - V_w = 450 \text{ Vdc}$
Voltages used in this measurement	$V_w = 320 \text{ Vdc}$, $V_b = 420 \text{ Vdc}$. $V_a - V_w = 340 \text{ Vdc}$, $V_a = -20 \text{ Vdc}$
Capacitance of each crosspoint	19 pF
Experimental conditions	0.15 NA of light excited in fibers Optical polarization: random at matrix entrance; TE and TM modes launched 2.6 collimation factor for fiber light 32 μW infrared source power 85 μm fiber core diameter 100 k Ω detector load resistance 0.4 Mbps optical data rate

MATRIX INPUT:
MODULATED SOURCES 1 AND 3

CROSSPOINT
ADDRESSING:



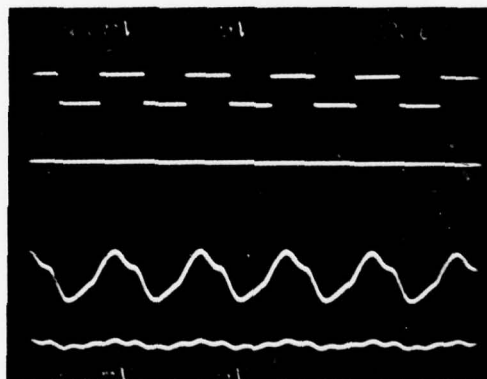
MATRIX
OUTPUTS:

CH. 4

CH. 6

CH. 4 ANALOG

CH. 6 ANALOG



CH. 4

CH. 6

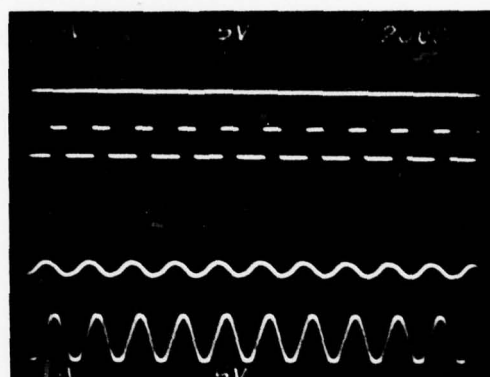
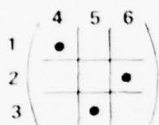
CH. 4 ANALOG

CH. 6 ANALOG

FIG. 55 Experimental performance of 3 X 2 fiber/matrix/fiber system (sample 8) excited by TE+TM 0.90 μm LED light, with terminals 1 and 3 transmitting. Digital and analog output signals are shown for two matrix configurations.

MATRIX INPUT:
MODULATED SOURCE 2 ONLY

CROSSPOINT
ADDRESSING:



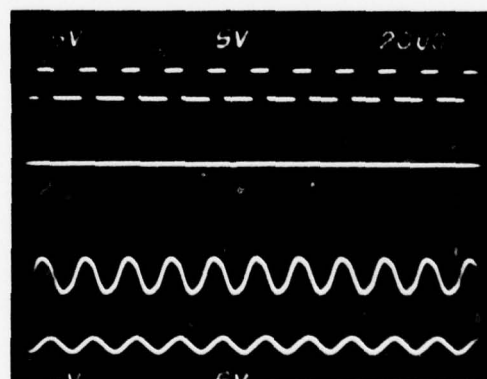
MATRIX
OUTPUTS:

CH. 5

CH. 6

CH. 5 ANALOG

CH. 6 ANALOG



CH. 5

CH. 6

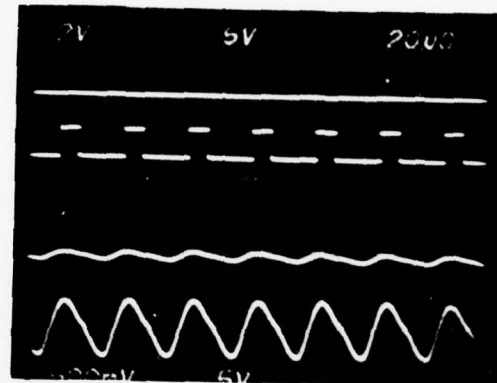
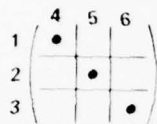
CH. 5 ANALOG

CH. 6 ANALOG

FIG. 56 Experimental performance of 3 X 2 fiber/matrix/fiber system (sample 8) excited by TE+TM 0.90 μm LED light, with terminal 2 transmitting. Digital and analog output signals are shown for two matrix configurations.

MATRIX INPUT:
MODULATED SOURCE 3 ONLY

CROSSPOINT
ADDRESSING:



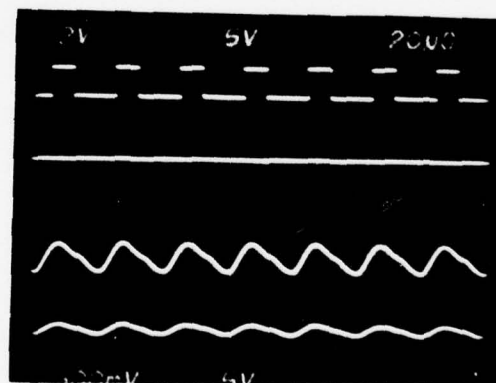
MATRIX
OUTPUTS:

CH. 4

CH. 6

CH. 4 ANALOG

CH. 6 ANALOG



CH. 4

CH. 6

CH. 4 ANALOG

CH. 6 ANALOG

FIG. 57 Experimental performance of 3 X 2 fiber/matrix/fiber system (sample 8) excited by TE+TM 0.90 μ m LED light, with terminal 3 transmitting. Digital and analog output signals are shown for two matrix configurations.

The angle-coupling of fibers appears practical. It was fairly easy to line up fiber arrays in the desired end-fire butt-coupling relation to the crystal's electro-optic channels, and the epoxy held the arrays accurately and permanently in place. Fiber/matrix coupling efficiency was high, as inferred from insertion loss-data, and the fiber spacing given by the microsaw grooves seemed sufficiently precise, although preferentially etched V-grooves would have given more accurate spacing.

The low 3 x 3 crystal-yield and the problems in the matrix crystal that remained (sample 8) prevented us from verifying simultaneous three-fold interconnects with all three LED terminals transmitting, although we did demonstrate the dynamic interconnection of two optical sources to various receivers. Three-fold hookups are, in our opinion, within the present state of the art.

The intermittency problems experienced with Sample 8 are not believed to be fundamental or characteristic features of these optical matrices. For example, Sample 9 had reproducible fiber/matrix interfaces despite its other problems. Extrapolating the present results, we think that a fully functional 9-element array can be made using present techniques, and that the signal and crosstalk levels would not drift.

Comparing the 3 x 2 experiment with theory, we feel the insertion loss result is in fairly good agreement with predictions because the discrepancy between the 19 dB observation and the 13.7 dB theoretical loss (Section 3) is attributable to low voltage levels in the 3 x 2 array, both the waveguide-bias and tapoff voltages. For example, in the related 2 x 2 result of Fig. 29, a 3 dB increase in switched throughput is found in going from $V_b=420$ V dc to $V_b=550$ V dc, thus 16 dB loss seems feasible in the 3 x 2 matrix.

Larger-scale switching matrices are possible by joining the present fiber matrices in multi-stage Clos-type networks, provided that the larger throughput losses are acceptable. For example, one could make a 12 x 12 crossbar, by assembling fiber-coupled matrices in three stages (See Fig. 4 of Ref. 2).

The optical crosstalk level, -8 dB average for the 3 x 2 matrix, was relatively high. However, since -10 dB was observed in some channels, we feel that a better-prepared 3 x 3 crystal would have a more uniform background level of -10 dB. If the TE-polarization could be filtered out in the angle-coupling process, one could trade off improved crosstalk performance for increased insertion loss.

It is difficult to establish theoretical guidelines as to what the multimode crosstalk should be. In an earlier theoretical discussion (Ref. 1), we noted that the input NA and output collection cone had an influence on "noise", although a more major role is played by the channel intersection angle. Taking an empirical approach, we would anticipate a crosstalk level of -40 dB for two electro-optic guides intersecting at 90° because this situation is analogous to the bulk-optic case (spectroscopic experiments, for example) where an optical background scattering level of 10^{-4} is found. In theory, a decrease in the intersection angle should increase the crosstalk.

Consistent with this, we observed a -25 dB optical extinction ratio in our compound crosspoint switch (Ref. 5) whose intersection angle was 5.8° . Similarly, going down to 3.6° as in the present crosspoints, we find crosstalk increases to -16 dB (and is -20 dB under low-NA conditions) for TM-polarized laser inputs. Of course, the fiber-coupling is a more severe test of crosstalk immunity because TE modes are present (in greater strength than TM modes because of the higher, off-normal Fresnel reflection coefficients) and these modes are confined only 50% as well as the TM modes, so the TE scattering can be sizable.

We do find consistency between the crosstalk results for 2 x 2 TM laser coupling and 3 x 2 TE+TM fiber coupling. Crosstalk is larger in the latter case for the following reasons: (1) the TE scattering mentioned above, (2) the low channel-bias voltage, set roughly 200 V dc below its optimum value, (3) the $(N-1)^{-1}$ dependence of scattering in an $N \times N$ array, (4) input fiber imperfections, chipping, misalignment, etc., and (5) crystal interface imperfections, like scratches, which are more noticeable in the latter case because the fiber excites a larger area than does the laser focal spot.

Like micro-optics, our multimode approach can integrate guiding and deflecting functions in one crystal. Unlike single-mode techniques, we use "thick films" rather than thin films and strong light trapping is automatically provided in the 75 μm direction. Our approach is not bulk-optic because the guide height is 75 μm rather than several millimeters. Our electro-optic approach is fast, achromatic, bidirectional, and does not rely upon mode interference.

Compared to the single-mode case, our voltages are one to two orders-of-magnitude larger because voltage is applied across the 75 μm guide dimension. While we get useful multimode modulation for 50 V applied, the "full" voltage is required to switch multimode light into an adjacent channel. At most 20% of the light can be transferred due to the $\Delta n \leq 1 \times 10^{-3}$ limitation. While we do not see a way to reduce the 400 to 500 V requirement at the electrical contacts to the LiTaO_3 switch, we note that low-voltage control sources can be used, either with miniature step-up transformers or with series-resonant circuits that we have tested for optical multiplexing.

Fiber light has been channeled here through a moderately complex network of multimode voltage-induced guides. The waveguide propagation losses here are low, about 0.3 dB/cm.

As a final comment, we wish to recall that these electro-optic matrices exhibit a temporary decrease in refractive index in crystal regions directly under the metal overlays with no voltage applied. This could be troublesome if measurements were made immediately after the device were built because performance specifications would be time varying. However, if one waits for two weeks, the passive effect will be completely gone and the matrix behavior will be perfectly reproducible.

14. SUMMARY AND CONCLUSIONS

Electro-optical matrix switching has been successfully demonstrated in a six-terminal fiber-optic communication system recently delivered to RADC/ET. Although the optical crosspoint yield was 78% on the

3 x 3 matrix (seven out of nine operative), all other aspects of the system worked well, including the direct angle-coupling of triple-fiber arrays to matrix input and output ports.

Keyboard-controlled switching of three independent randomly polarized infrared data streams from 0.90 μm GaAs LEDs have been demonstrated, and various conversations between fiber-linked terminals have been selected.

The matrix mates to commercial fibers, each transmission line being a single strand of low-loss Corning all-silica 0.15 NA multimode fiber. The system will work with graded or step index fibers, 50 to 85 μm core diameter, and the system performance specifications would be better than reported here if a fiber-NA less than 0.15 were chosen, for example 0.10.

Since the matrix and fibers do not radiate information into their surroundings, the intercom is secure. And the system reliability is enhanced because signals are not converted to the electrical domain for switching, with subsequent re-conversion.

Two "firsts" were achieved on this contract: the 2 x 2 array is the first multimode electro-optic matrix reported in the literature, and the 3 x 2 fiber-coupled crossbar is the first multimode fiber-optic switch of its kind.

Early in the contract, good results were found in individual crosspoints and 2 x 2 arrays, but construction problems arose later in going to 3 x 3 arrays. The chief problems were the vulnerability of the insulating film (electrical crossover layer for crosspoints) to environmental factors and the fragility of larger crystals.

The present LiTaO_3 - LiNbO_3 crystal growth art limits the size of optical quality 3-mil z-cut plates to 7 cm x 1 cm. Given these materials and sizes, a serious drawback of the present electro-optic approach is that it does not appear expandable to medium scale (10 x 10) and large scale (100 x 100) monolithic arrays. On the positive side, however, we believe that a 4 x 3 switching array can be built on such a plate with our techniques.

Although large by some standards, the observed 19 dB optical insertion loss of the addressed 3 x 2 matrix is taken only once in the system. Generally, such losses will be acceptable in many applications if the switch occupies a central location in the network. Our system, with 32 μ W inputs, had adequate output levels.

The optical crosstalk found in the 3 x 2 fiber/matrix/fiber combination, approximately -8 dB, is high, although not vastly different from that found in related "real world" multimode fiber-coupled systems, such as the 4:1 optical multiplexer of Ref. 3. Optical background levels of this order can be handled with signal-processing comparator circuits in the receivers that "clean up" detected bits and restore those pulses to 1 levels.

If the matrix were to be switched in microseconds or nanoseconds, the high-voltage control (400 to 500 V) would require considerable reactive power. If, however, the matrix is configured at slower rates, as is usually the case, these voltages can be handled easily with appropriate transistors or with pulse transformers.

In this context, we should point out the distinction between the optical bit rate and the matrix switching rate. Frequently, the matrix will be called on to perform packet switching or message handling. Here, the configuration rate is orders of magnitude below the optical information rate. And, the matrix does not in any way degrade the wideband (> 100 Mbps) data-handling rate of the fibers.

15. RECOMMENDATIONS FOR FUTURE WORK

Due to inoperative crosspoints mentioned above, gaps exist in our knowledge of the 3 x 3 crossbar properties; thus, it would be worthwhile to carry out performance measurements on a fully functional array. Useful information could also be gained by examining 4 x 3 arrays that we believe are feasible on 7-cm LiTaO_3 plates.

Our main recommendation is that crossbar improvements should be made within the present electro-optic approach, and in modified approaches discussed below.

Technology improvements and performance improvements are available in the electro-optic realm. A prime area for further work is the technique for contacting the tops of the various crosspoints. One possible approach that eliminates the 60 μm resist layer is to make electrical contact to the 1-mil crosspoint bars by attaching 1-mil-diam gold wires to the bars (manually) with 1-mil-diam dots of gold conductive epoxy. Then, for further protection, the wire-bonded assembly could be immersed in an insoluble, insulating "potting compound". Another approach would be to paint gold-epoxy paths into 1-mil-diam holes in a glass plate that covered all of the top-surface metalizations.

The present processing could be upgraded to meet military temperature-range specifications. This could probably be done by substituting an epoxy or other non-melting cement for the thermally softenable paraffin or glycolphthallate.

More insight is needed into the metal-overlay effect. We discussed previously the zero-voltage index-decrease produced by metal overlays on LiTaO_3 . It would be desirable to gain a better understanding of this passive effect and to eliminate it in future crossbars (or to stabilize the effect and put it to use).

With regard to crossbar performance, a 33% reduction in voltage is attainable by changing to a 50 μm plate (the minimum thickness that can be handled at present) which is compatible with 50 to 60 μm -core-diameter fibers.

Very significant performance improvements would come about if (and it is a big if) improved electro-optic materials became available. To get an idea of what we mean, consider the crossbars that could be made if optical quality crystals, 7 cm x 1 cm x 75 μm , with r-coefficients ten times larger than those of LiTaO_3 could be purchased. Using our present techniques, we could make channels, smaller in cross-section than 225 x 75 μm , that would confine a larger numerical aperture of light and that would allow near-normal-incidence coupling of fibers to the matrix (a low collimation factor). Also, we could use larger channel-intersection

angles, resulting in less background light and allowing shorter crosspoints, thereby making possible larger-scale matrix arrays on the given crystal area. Sad to say, few laboratories are engaged in the materials quest, so it is quite unlikely such a material will be produced. Failing this, there are other avenues that can be pursued, for instance, combining the present electro-optic effect with passive, ion-diffused waveguides.

Significant improvements can be gained by substituting passive channels for the guides now created by continuous application of a bias voltage. For example, deep multimode channels have been made by thermal indiffusion of copper ions into LiNbO_3 (Ref. 1) and the NA of light confined can be large if the ion doping density is large, although there is a trade-off between the ion concentration and the waveguide propagation loss. Most importantly, the use of diffused channels eliminates the possibility of voltage breakdown between wall- and crosspoint-electrodes, and gives equal guiding of both light-polarizations.

For matrixing, we suggest a set of doped channels in a single-crystal substrate of LiNbO_3 or LiTaO_3 . The guides intersect one another or make a series of close approaches (e.g., 50 μm separation), thereby permitting voltage-controlled multimode coupling (tapoff switching) between channels by means of the conventional Pockel's effect which is retained in the diffused crystal. Localized sets of surface electrodes at guide crossings are used for switching.

If suitable dopants are found, light with relatively high NA will be trapped (with the attendant benefits mentioned above). In this connection, large index-increases have been found (R. V. Schmidt, BTL) in the high-temperature diffusion of ZnO into LiNbO_3 , and the multimode channels are colorless (low-loss), unlike the yellow-orange copper-doped guides that have relatively high attenuation.

We also suggest extending our optical matrix approach to the use of electro-optic liquid crystals, such as the nematic fluids now offered commercially. The idea here is to use the liquid crystal as a controlled coupling medium between various passive multimode waveguides. A thin layer

of liquid crystal will act as a voltage-controlled waveguide cladding if it is placed between two waveguide cores whose core index is midway between the liquid's ordinary and extraordinary indices. The liquid crystal is highly voltage-sensitive, and a small potential will produce a significant alteration of its refractive index in the TE and/or TM-mode direction. Various arrangements of crossed guides and electrode layouts will do the desired $N \times N$ switching.

REFERENCES

1. R. A. Soref, "Optoswitch Crosstalk Study", Final Report on Contract No. F30602-76-C-0129, Rome Air Development Center, Griffiss Air Force Base, New York 13441, March 1977. (Sperry Contract Report 77-22), A044208.
2. M. J. Marcus, "The Theory of Connecting Networks and Their Complexity: A Review", Proc. IEEE, 65, 1263 (1977)
3. A. R. Nelson, "Multiplexing and Filtering of Optical Signals", Final Report on Contract No. DAAB07-76-C-1343, U.S. Army Electronics Command, Fort Monmouth, New Jersey 07703, June 1977. (Sperry Contract Report 77-40).
4. R. A. Soref, "Compound Optical Crosspoint with Low Crosstalk", Applied Optics, 16, 3223, (Dec 1977)
5. R. A. Soref, "Properties of the Terminated Optical Crossbar Matrix", Applied Optics, 15, 2950 (Dec 1976).
6. R. A. Soref and D. H. McMahon, "Multimode 2 x 2 Optical Crossbar Switch", Electronics Letters, 14, 283 (1978).
7. Quarterly Status Reports have been issued on this contract as follows: QSR-1, Sept 15, 1977, Sperry Research No. CR-77-61; QSR-2, Dec 15, 1977, SRN-CR-77-85; QSR-3, March 15, 1978, SRN-CR-78-13.

APPENDIX A

DEVICE PROCESSING PROCEDURE

A. Initial Clean-up

The 3.1-mil-thick undoped LiTaO_3 plate, 2.625" x 0.500", optically polished on both large faces, was received from Crystal Technology Inc., Mountain View, Calif. In shipment, the plate was glued to a 3" x 1" glass microscope slide with paraffin wax. Before working the crystal, the crystal and slide are heated to 120°C and any air bubbles in the paraffin under the crystal are squeezed out by gently pressing on the crystal with a wooden probe. Care must be taken during processing not to subject the crystal to sudden temperature changes.

After a slow cool-down, the exposed crystal surface is cleaned. The sample is placed in a Petri dish filled with acetone and allowed to soak for 30 sec. Slight agitation by hand aids in washing away remaining paraffin. Using an acetone-soaked cotton swab, the last paraffin is washed away. This takes several swabs. There are no visible streaks on the crystal. Some undercutting of the crystal occasionally results. If so, the sample is reheated to 120°C to reflow paraffin out to the crystal edges. Then the sample is cooled slowly.

The sample is placed in a beaker of Micro detergent solution (one tablespoon, plus 400 ml deionized filtered water). The sample is agitated by hand for 30 sec to remove ionic contaminants on the crystal. It is rinsed thoroughly with running filtered water (Barnstead ultrapure filter) and is blown dry with 4-micron-filtered air. The entire crystal face is stroked with a cotton swab soaked in Decontam cleaning agent, then rinsed and blown dry.

B. Photolithography - First Side

Photoresisting is done in a clean hood under Yellow lighting. The sample is placed on the spinner, and the entire area is covered with Shipley AZ 1350B positive photoresist (previously passed through a 4-micron filter). The sample is spun at 5000 rpm for 20 sec, which produces a 2000-Å-thick resist layer. Build-up of resist on the crystal edges is minimized by covering the entire surface initially. The sample is dried in a dust-free box at room temperature for 30 minutes.

The mask (e.g. 3x3-2) is thoroughly cleaned with acetone, trichlorethylene, and DI water, each in the ultrasonic bath. It is blown dry with filtered air. The sample and mask are placed in the alignment fixture, with the mask making intimate contact to the crystal. (If interference fringes are not observed, the edge build-up of resist is exposed-off prior to pattern exposure).

When intimate contact is obtained, the photoresist is exposed using a 200 W mercury arc lamp for 30 seconds. Then the sample is removed and developed for 10 sec in Shipley developer; then rinsed and blown dry. With a 100x microscope, the pattern is inspected for sharp edges and complete resist removal where desired.

The sample is placed (upside down) in an evaporator equipped with a chromium rod source and a gold boat source. Vacuum to 1×10^{-6} Torr is pulled, and 50 Å of Chromium is deposited, followed by a 700 Å evaporation of gold onto the sample. These thicknesses are less than the photoresist layer thickness, which facilitates liftoff and gives ample metal for conduction.

The sample is immersed in an acetone-filled Petri dish and hand-agitated for 25 sec until metal has lifted off the resist areas. The sample is removed and immediately placed in a bath of filtered water to prevent rapid evaporation of acetone which can cool the crystal too quickly. The sample is then removed and allowed to dry. After microscopic inspection, if some metal flecks are still attached, they are removed by gentle wiping of the area with an acetone-soaked swab.

C. Turning the Crystal Over for Access to Side "B"

A second glass substrate (the final one) is prepared by making a small U-shaped cutout in the middle (Fig. 35) for electrical access to the side-A pattern (the "ground side" of the crystal is later slid over this cutout). This microscope slide is cleaned with acetone and placed on a hot plate. The electroded sample is also put on the same hot plate and heated to 120°C. When that temperature is reached, the entire electroded surface is covered with glycol pthallate.

Gylcol pthallate, also known as Crystalbond 509, is a clear insulating cement that melts at about 100°C and becomes workable (low viscosity) at 120 to 125°C.

The loosened crystal is slid to the edge of the old slide with a wooden stick. GP is put on the central area of the new slide and the hot plate temperature allowed to rise to 150°C, making the GP quite "runny". Using tweezers, the old slide-plus-crystal is turned over and placed on the new slide with the crystal near one edge of the latter. After standing for 2 minutes, the top glass (old slide) is slid off completely, gently and slowly. (The hot plate temperature is monitored and not allowed to exceed 155°C). When the top glass has been removed, the crystal is centered in the new slide (not over the cutout yet). Using a wooden probe and gentle pressure, any air bubbles under the crystal are squeezed out. The sample is removed from the heat and cooled slowly. Side B is now accessible, and the initial clean-up process is now repeated.

D. Photolithography - Second Side

Photolithography on side B is done in the same way as on the crystal's first side (Section B above). The side B electrode pattern (e.g. Mask 3x3-1), which is what we have referred to previously as the top electrode pattern) is registered (with the aid of a microscope) on the crystal directly over the bottom electrode pattern done earlier. Metalization and liftoff are as before.

E. Insulating Layer

The high-viscosity resist, Shipley AZ 1350 J (filtered with a 4-micron filter) is used for the insulating film. On the spinner, the electroded crystal (on its slide) is saturated with resist and spun at 1800 rpm for 20 sec. It is air-dried in a dust-free box for 20 min. This spinning-and-drying process is then repeated six more times. After seven layers have been applied, the overall thickness is approximately 60µm as indicated by microscope depth-of-focus measurements. Excess photoresist is removed from the glass slide, from the perimeter of the crystal, from a 1/8" band on the long edges, and from 1/4" bands at the crystal ends.

F. Windows

The window mask (e.g. Mask 3x3-3) is carefully aligned over the 1-mil-wide crosspoint vanes so that the 0.9-mil-wide openings are centered in those vanes. Contact printing is then done. The ultra-thick resist is first exposed to UV for 80 sec, developed for 10 sec in the Shipley solution, rinsed in DI water, and blown dry. Then (after putting the sample in the mask aligner) the expose-and-develop cycle is repeated two more times (a total of three exposures) which is necessary to penetrate the resist. Inspection with a 100x microscope is done to ensure that the windows go all the way through the layer and that "naked" metal is seen. The sample is placed in an oven and the temperature raised slowly, over 60 min, to 125°C where it is held for two hours. This bakes and hardens the thick resist, driving out moisture, thereby preventing out-gassing and bubbling from occurring during future processing steps. Over 20 min., the sample is cooled to room temperature.

G. Protective Glass Pieces

Three small pieces of glass are glued to the top surface, two for sawing protection and one for "cutout" protection. (See Fig. 35) For the latter, the sample is put on the hotplate, heated to 120°C, and slid with a wooden probe until the bottom electrode is over the glass opening. (the probe touches the resist edge, not the crystal edge). A preheated piece of glass 3/8" x 3/8" x 1/16" is placed on the "naked" crystal using tweezers. In the same manner, glass pieces 1/8" x 5/8" x 1/16" are installed on the crystal ends covering the unresisted 1/4" wide areas. This top-and bottom glass sandwich prevents crystal cracking during the subsequent sawing operation. Care is taken to keep the window areas clean during this operation. Then the sample is slowly cooled to room temperature.

H. Conductive Paths

As Fig. 34 indicates, the electrical paths to the crosspoints go down (60 μ m) into a "valley" and must go around a "corner" of the insulator in so doing. This requires an angle-evaporation of metal to maintain a continuous path.

The metal evaporation mask (e.g. Mask 3x3-4) made from 5-mil molybdenum, is just large enough to "settle down" on the crystal between the protective glass pieces. Using a microscope, the mask is aligned over the windows, taking care not to scratch the resist during the line-up. Small pads of masking tape hold the mask in place, and tape also covers all remaining glass areas. The mask-crystal assembly is put in the vacuum chamber with the crystal plane oriented at 70° to the source, rather than the usual 90° . This tilting enables the outcoming metal to bombard both the "corner" and the "hillside" of the insulator-opening, thereby depositing an unbroken metal path. At 1×10^{-6} Torr, 100 Å of Cr is applied, followed by a 1000 Å gold deposition in the same pump-down. The sample is removed, tape removed, and gold paths examined for continuity.

I. Cutting and Polishing

A ceramic block, heated to 120°C is covered with GP, and the preheated sample is put on this melted cement and allowed to cool. The block then sits in a rotatable brass goniometer jig that is set at the desired 39° angle. Using an automatic wafer-cutting machine, the crystal sandwich is cut with the 10-mil-wide, 100 grit, 3"-diameter diamond wheel saw. Cutting is done slowly at .045" per minute. Then the jig is set to the appropriate angle for the other end of the matrix, and the second cut is made. The sandwich is removed from the ceramic block and cleaned with acetone.

Polishing is done in four stages with the following abrasives: 600 grit paper, 12-micron paper, 4-micron paper, and Syton. Each step is done by hand using a motor-driven 10"-diameter polishing wheel. The final Syton step uses a felt polishing pad. At each stage, the polishing is continued until the finish has the degree of perfection associated with the particular grit size being used. Both ends of the matrix are polished flat for direct end-coupling to fibers. To get reproducible, flat ends, the sandwich is held against a square glass block that holds it perpendicular to the polishing wheel.

J. Electrical Contact

Contacts to the sample are made using Acme Conductive Adhesive (E-solder number 3025, a two-part epoxy). Using acetone and a cotton swab, GP is cleaned out of the ground contact-pad, then epoxy is added and trailed over the remaining GP and onto the glass, where a flexible #26 gauge tinned wire is inserted in the conductive

trail. Similarly, for the top ten contacts, epoxy trails are made, going from the gold paths to the glass substrate, where the same thin wires are attached. After the adhesive cures, the matrix sandwich is cemented with tiny Torr-seal epoxy dots to a triangular glass mounting base.

APPENDIX B

BIBLIOGRAPHY

Many of the ideas and techniques described in this Report are discussed at greater length in related Sperry publications. We therefore append here a complete list of Sperry Research Center publications in multimode optics, an endeavor that began in 1974.

1. R. A. Soref, "Integrated-optic matrix switch design" presented at the DoD Integrated Optics and Fiber Optics Communications Conference, San Diego, CA, 17 May 1974.
2. R. A. Soref and A. R. Nelson, "Thick-film optical switches", presented at the ONR-ARPA Program Review, Washington, D.C., 24 February 1975.
3. R. A. Soref, "Crosstalk reduction in optical switching" *Applied Optics*, 14, 2559, November 1975.
4. D. H. McMahon, "Efficiency limitations imposed by thermodynamics on optical coupling in fiber-optic data links", *J. Optical Society Am.*, 65, 1479, December 1975.
5. A. R. Nelson and R. A. Soref, "Properties of a multimode electro-optic polarization switch for fiber optics", presented at the OSA annual meeting, Boston, MA, 24 October 1975.
6. A. R. Nelson, "Coupling optical waveguides by tapers", *Applied Optics*, 14, 3012, December 1975.
7. D. H. McMahon and R. L. Gravel, "Distributive tee couplers", *Applied Physics Letters*, 28, 396, 1976.
8. A. R. Nelson, D. H. McMahon and R. L. Gravel, "Electro-optic channel waveguide modulator for multimode fibers", *Applied Physics Letters*, 28, 321, 1976.
9. H. van de Vaart, "Surface acoustic wave multiplexed optical data link", Sperry Research Paper 76-29, May 1976.
10. R. A. Soref, D. H. McMahon, and A. R. Nelson, "Multimode achromatic electrooptic waveguide switch for fiber-optic communications", *Applied Physics Letters*, 28, 716, 1976.

11. A. R. Nelson and D. H. McMahon, "Modulators for multimode single-fiber communications systems", presented at the Electrooptic Systems Design Conference, New York, NY, 14 September 1976. Proceedings of Tech. Program, pp 36-39.
12. H. Wichansky, L.U. Dworkin, and D. H. McMahon, "Multimode optical devices for signal processing", presented at the EOSD Conference, New York, 15 September 1976., *ibid*, pp 581-586.
13. R. A. Soref and A. R. Nelson, "Electro-optic multimode multiplexer", presented at the Int'l. Electron Devices Meeting, Washington, D.C., 7 December 1976. Tech. Digest, pp 229-231.
14. R. A. Soref, "Properties of the terminated optical crossbar matrix", *Applied Optics*, 15, 2950, December 1976.
15. D. H. McMahon and R. L. Gravel, "Star repeaters for fiber-optic links", *Applied Optics*, 16, 501, 1977.
16. A. R. Nelson and R. A. Soref, "Electro-optic polarization-switch for multimode fibers", *Applied Optics*, 16, 119, 1977.
17. A. R. Nelson, D. H. McMahon, and R. L. Gravel, "Electro-optic multiplexer for large-numerical-aperture low-loss fibers", *Optics Letters*, 1, 35, July 1977.
18. D. H. McMahon and A. R. Nelson, "Device and system concepts for multimode single-fiber optical data links", presented at the AGARD Conference on Optical Fibers, London, England, 16 May 1977.
19. A. R. Nelson and R. A. Soref, "Active components and system concepts for multiterminal fiber optic data links", presented at INTELCOM 77, Atlanta, GA, 14 October 1977. Exposition proceedings, vol.2, pp. 694-698.
20. R. A. Soref and A. R. Nelson, "Compound optical crosspoint with low crosstalk", *Applied Optics*, 16, 3223, December 1977.
21. R. A. Soref, A. R. Nelson, D. H. McMahon, W. B. Spillman, Jr., and L. E. Sheppard, "Active fail-safe terminal for fiber-optic data bus", *Applied Physics Letters*, 32, 408, April 1978.
22. R. A. Soref, "Optical switching and data distribution", presented at the New England Chapter, Optical Society of America, Sturbridge, MA, 18 May 1978.
23. W. B. Spillman Jr., R. L. Gravel, and R. A. Soref, "A fiber-optic data bus using active fail-safe terminals", presented at Electro-optics Laser Conference, Boston MA, 20 September 1978.

24. W. B. Spillman Jr., R. L. Gravel and R. A. Soref, "A fail-safe fiber-optic data bus using active multimode mirror terminals", Applied Optics, 17, 1978.
25. R. A. Soref and D. H. McMahon, "Multimode 2 x 2 Optical Crossbar Switch", Electronics Letters, 14, 283, 1978.
26. R. A. Soref, "Multimode switching components for multi-terminal links", presented at the Annual Symposium, Society for Photo-optical Instrumentation Engineers, San Diego, CA, 29 August 1978.
27. D. H. McMahon and R. A. Soref, "Multimode optical multiplexing with low-voltage drivers", Optics Letters, 2, 1978.

CONTRACT REPORTS (FINALS ONLY)

1. R. A. Soref and L. R. Schissler, "Optical switch study" Final Report on Contract No. F30602-74-C-0168, Rome Air Development Center, Griffiss Air Force Base, New York 13441, October 1974, A007009.
2. R. A. Soref, A. R. Nelson and D. H. McMahon, "Integrated optical switches", Final Report on Contract No. N00014-74-C-0321, Office of Naval Research, Arlington VA 22217, July 1975.
3. R. A. Soref, "Optoswitch crosstalk study", Final Report on Contract No. F30602-76-C-0129, Rome Air Development Center, Griffiss Air Force Base, New York 13441, March 1977, A044208.
4. A. R. Nelson, "Multiplexing and filtering of optical signals", Final Report on Contract No. DAAB07-76-C-1343, U.S. Army Electronics Command, Fort Monmouth, NJ 07703, June 1977.

A decorative rectangular border with a repeating scroll-like pattern surrounds the central text.

MISSION of Rome Air Development Center

RADC plans and conducts research, exploratory and advanced development programs in command, control, and communications (C³) activities, and in the C³ areas of information sciences and intelligence. The principal technical mission areas are communications, electromagnetic guidance and control, surveillance of ground and aerospace objects, intelligence data collection and handling, information system technology, ionospheric propagation, solid state sciences, microwave physics and electronic reliability, maintainability and compatibility.